2016

Mechanistic Studies of the Structure-Photostability Relationship of Organic Conjugated Polymers

Logan Paul Sanow
South Dakota State University

MECHANISTIC STUDIES OF THE STRUCTURE-PHOTOSTABILITY RELATIONSHIP OF ORGANIC CONJUGATED POLYMERS

BY

LOGAN PAUL SANOW

A dissertation submitted in partial fulfillment of the requirements for the

Doctor of Philosophy

Major in Chemistry

South Dakota State University

2016

MECHANISTIC STUDIES OF THE STRUCTURE-PHOTOSTABILITY RELATIONSHIP OF ORGANIC CONJUGATED POLYMERS

This dissertation is approved as a creditable and independent investigation by a candidate for the Doctor of Philosophy in Chemistry degree and is acceptable for meeting the dissertation requirements for this degree. Acceptance of this does not imply that the conclusions reached by the candidate are necessarily the conclusions of the major department.

Cheng Zhang, Ph.D. _____ Date
Dissertation Advisor

Douglas Raynie, Ph.D Date
Head, Department of Chemistry and Biochemistry

Dean, Graduate School Date

ACKNOWLEDGEMENTS

I would first like to thank my advisor, Dr. Cheng Zhang for believing in me, guiding me throughout my studies, and always being available to his grad students. I would also like to thank the members of my graduate committee; Dr. Fathi Halaweish, Dr. Brian Logue, Dr. Qiauan Qiao, and Dr. David Clay, for your time and guidance.

I would like to thank my group members Manik Gudimani, Aubrey Jones, Eric Nagel and Dan Liu. I would specially like to thank Dr. Jianyuan Sun with whom I've worked closely with on many of the projects. I would also like to thank Dr. Lianjie Zhang who taught me techniques when I was first joining the Zhang group.

I am grateful for the support I have received from South Dakota IGERT (the National Science Foundation Grant No. 0903685) the past two years and for the opportunities that the program has given me. It has helped me become a better science communicator and has given me the tools to be successful in my career. I am also thankful for the financial support from the U.S. Air Force Office of Scientific Research (Award No. FA955010-1-0555), the National Science Foundation/SD EPSCoR (Award No. 0903804)

I am extremely thankful to have completed my graduate work close to my family, they have always been there to support me. I specifically want to thank my parents, Mr. Marvin (Louie) Sanow and Mrs. Mary Jo Sanow. They have always supported my aspirations and they are a big reason that I have been able to accomplish what I have.

Most of all I am thankful for my wife Stefanie, she has been with me every step of the way, offering love and encouragement, I couldn't have done it without her.

CONTENTS

LIST OF FIGURES

LIST OF SCHEMES

LIST OF TABLES

ABSTRACT

MECHANISTIC STUDIES OF THE STRUCTURE-PHOTOSTABILITY RELATIONSHIP OF ORGANIC CONJUGATED POLYMERS

LOGAN PAUL SANOW

2016

Organic Conjugated polymers (CPs) are a subject of intense research for their application in organic photovoltaics (OPVs), organic light emitting diodes (OLEDs), solid-state dye lasing, biological imaging and sensing, chemical sensing and remote sensing. CPs are key materials in the quest for more sustainable forms of renewable energy, making electronics more versatile and light weight, and increasing the functionality of everyday materials. For these applications and others that use CPs as the photoactive material, one of their main drawbacks is their susceptibility to photodegradation. Photodegradation occurs when the material is exposed to light leading to irreversible changes in the materials, most often resulting from photoxidation. These irreversible changes cause loss of mechanical, electronic and photophysical characteristics. For practical applications of CP devices, lifetime is as important as device efficiency. The following research is focused on studying the photodegradation mechanisms in various CPs to better understand the relationship between structure and stability, which may lead to the design of CPs which are more intrinsically photostable.

To study how dependent photostability is on a polymer's chemical structure and frontier orbital energies, two series of CPs were studied. The first series contained two dicyano-substituted polyphenylenevinylene polymers with different side chains: poly(2,5-

dioctyl-1,4-phenylene-1,2-dicyanovinylene) (C8-diCN-PPV) and poly(2,5-bis(decyloxy)-1,4-phenylene-1,2-dicyanovinylene) (RO-diCN-PPV). The second series included a well-known polymer, poly(3-hexylthiophene) (P3HT), and a newly synthesized CP, Poly(3,5-didodecyl-cyclopenta[2,1-b;3,4-b']dithiophen-4-one) (C6-CPDTO). The photodegradation mechanisms were studied through a combination of UV-Vis, PL, FTIR and NMR spectroscopy as well as gel permeation chromatography. There are two main degradation mechanisms that lead to photodegradation of CPs, the radical mechanism is initiate by generation of superoxide radical anion and the other mechanism is initiated by singlet oxygen.

C8-diCN-PPV has a lower LUMO level compared to RO-diCN-PPV, yet photodegrades more quickly. RO-diCN-PPV and C8-diCN-PPV both photodegrade through a singlet oxygen mechanism. If DABCO, a singlet oxygen quencher, is introduced into the diCN-PPV polymer films, DABCO induces a radical degradation in RO-diCN-PPV and quenches the singlet oxygen degradation in C8-diCN-PPV.

C_6-CPDTO contains a fused ring monomer with an electron withdrawing ketone unit that lowers the LUMO level compared to P3HT. C6-CPDTO also contains half the number of side-chains, compared to P3HT, per structural unit; side-chains are a known weakness of a polymer's photostability. It was observed that P3HT and C_6-CPDTO degrade by radical degradation, while P3HT also degrades somewhat by singlet oxygen. The findings show that the mechanism by which a particular CP photodegrades is determined by a combination of the electronic and photophysical characteristics of a polymer.

Chapter 1 Introduction to Conjugated Polymers and Photochemical Degradation Mechanisms

Conjugated Polymers (CPs) are polymers having π-electron conjugation along the polymer main chain. Conjugation occurs when the main chain consists of alternating double and single bonds. Conjugation gives these polymers electronic and optical characteristics that make them semiconducting and optically active. CPs have been the focus of intense research interest for their application in Polymer Solar Cells (PSCs)[1-2], Organic Field Effect Transistors (OFETs)[3-4], Organic Light Emitting Diodes (OLEDs)[5-7], Solid-State Dye Lasing,[8-9] Biological Imaging and sensing,[10-14] Chemical Sensing[15-18] and Remote Tracking. Even though there has been a concerted effort to increase the performance of devices that utilize conjugated polymers, little research has investigated the photostability of conjugated polymers

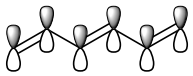

Figure 1.1 Alternating π and σ bonds creating a conjugated system.

1.2 Conjugated Polymers

Conjugated polymers possess a variety of unique characteristics due to the delocalization of their electrons. Delocalization indicates that the electrons are not confined to one orbital, instead a conjugated polymer's wave function is spread over the entire conjugated system. Delocalization of the electrons gives rise to charge carrier mobility which increases the conductivity of the polymer. Organic Polymers are traditionally seen as being non-conductive, which is why polymers are commonly used as insulators on wires and in electronic devices. In the 1800s it was observed that a natural

insulator, rubber, could be made more conductive through the addition of carbon black. In 1862, Henry Letheby showed that anodic oxidation of aniline in sulfuric acid produced a conductive material.[19] This conductive material most likely was polyaniline, Figure 1.2. Polyaniline is a good example of the effects that conjugation has on the properties of a polymer. In Figure 1.3, 3 different oxidation states of polyaniline are shown- leucoemeraldine; at the lowest oxidation state; is not conjugated and appears as a colorless solid with low conductivity. As polyaniline is oxidized to emeraldine, the color turns to a green-blue color and conductivity increases. With additional oxidation, the polymer becomes (per)nigraniline which is violet and conductive.[20] In the 1930s, natural rubber filled with acetylene black was commonly used in hospitals to control the buildup of static electricity. Prior to 1973, the only known conjugated polymer with any appreciable conductivity was polysulfurnitride $(SN)_n$. Heeger, MacDiarmid and Shirakawa (1977) showed that an Organic Conjugated Polymer (polyacetylene) doped with Iodine[21] had conductivity comparable with inorganic materials, these researchers would later receive the Nobel Prize in Chemistry in 2000[22] for their work on conjugated polymers. Since this time, research into conjugated polymers has been very intense, particularly in the past two decades. Depending on theseparation between energy levels shown in Figure 1.4, These organic polymers can be insulating, conducting or semiconducting**.** In inorganic semiconductors, the energy levels are called the valence and conducting bands. They are referred to as bands in inorganic semiconductors, the atoms have a uniform lattice, resulting in energy levels that overlap to form bands in which electrons can occupy. In organic materials, we often describe photophysical processes taking place on an individual molecule, this is because the electrons do not

flow easily between molecules, and instead they “hop”. The energy level in organic materials that is analogues to the valence band is called the Highest Occupied Molecular Orbital (HOMO). This is the highest energy orbital where electrons are found at the ground state. The energy level that corresponds to the conducting band is called the Lowest Unoccupied Molecular Orbital (LUMO), this orbital is the next highest energy orbital after the HOMO, it contains no electrons in the ground state. The Singly Occupied Molecular Orbitals (SOMOs) are the highest energy molecular orbital to contain an electron, but they only contain one electron as opposed to a pair of electrons, in this sense they are a combination of the HOMO and LUMO of a molecule, as it both contains an electron but also can accept an electron. The energy gap that determines whether a material is insulating, conducting, or semiconducting is determined by the difference in energy between the LUMO and HOMO levels.

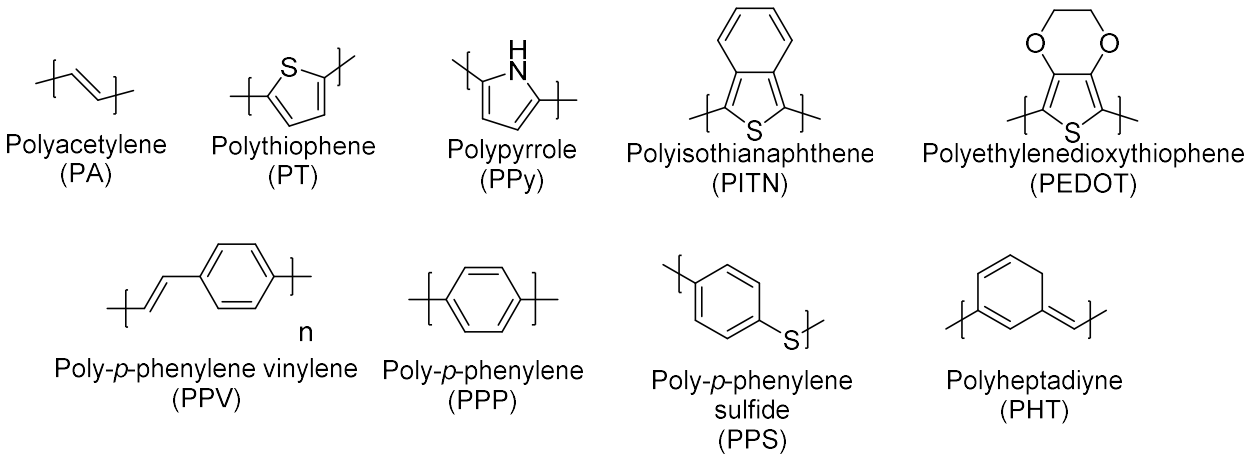

Figure 1.2 Examples of commonly used conjugated polymers.

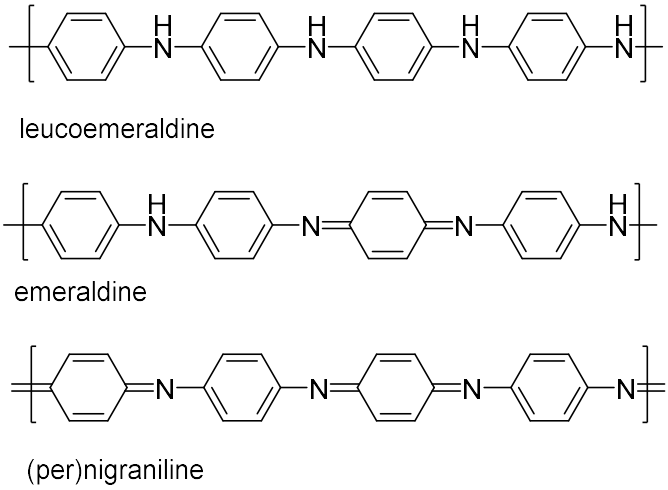

Figure 1.3 Polyaniline, the first conjugated polymer, in its various oxidation states. Conductivity increases from leucoemeraldine<emeraldine<(per)nigraniline.

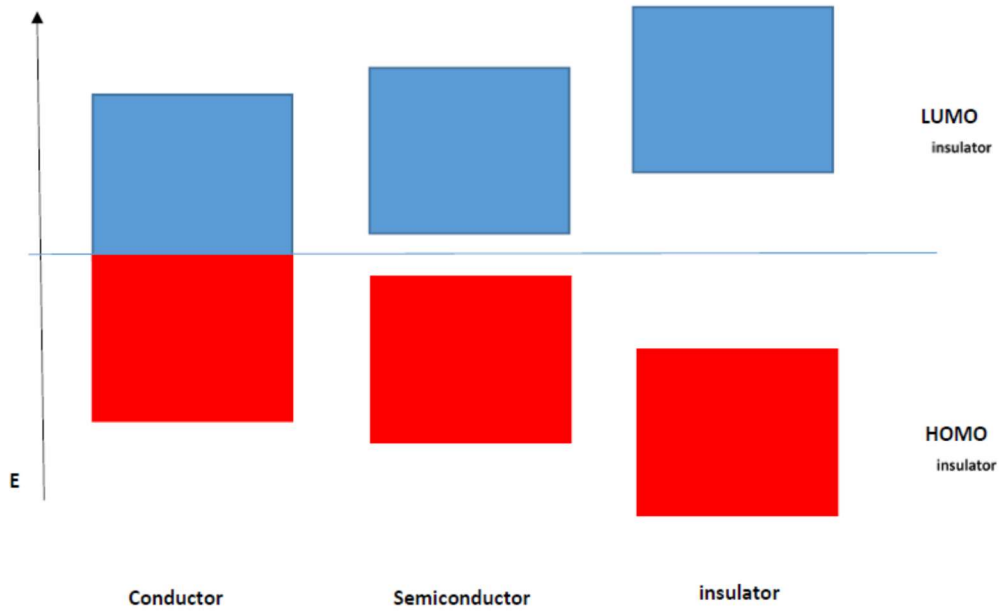

Figure 1.4 Relative bandgaps of conductors, semiconductors and insulators.

1.3 Electronic and Optical Processes in Conjugated Polymers

The delocalization of electrons in the backbone of the polymer allows for the LUMO and HOMO to be closer together, reducing the energy gap between them. Electrons can undergo electronic transitions between the HOMO and LUMO levels. These electronic transitions are typically caused by light. When light incident on the conjugated polymer is of an energy that is equal to or greater than that of the band gap, the polymer will absorb a photon through the excitation of an electron from the HOMO to the LUMO. This promotion of an electron also creates an associated hole. The electron in the LUMO and the hole in the HOMO are delocalized over the conjugated system of the polymer. In order for the electrons to move through the bulk material, they must undergo a transition between polymer chains. These transitions occur through two different processes, typically the electrons hop between polymer chains to move through the bulk material. Less often the electrons will move through the material through a quantum tunneling mechanism. The mechanism by which the electrons move through the bulk material is dictated by a number of factors including thickness of the bulk material, defects, film morphology and temperature.[23]

Optically the CP can undergo a number of different processes, including absorbance, fluorescence, and phosphorescence. Absorbance, as mentioned earlier is when light with energy that is equal to or greater than that of the band gap, the material will absorb the light through excitation of an electron. From the excited state an electron can relax to the ground state through various pathways. The first pathway is non-radiative decay, this occurs through the loss of phonons, vibrational energy in the bulk material. The second pathway is fluorescence, in which an electron from the excited state relaxes to the ground state through the emission of a photon that is equal in wavelength to the

energy of the bandgap. The third pathway is phosphorescence, in which an electron from the excited state undergoes intersystem crossing to an excited triplet state. This triplet state contains an excited electron with an inversed spin. The inversion of spin prevents the electron from relaxing to the ground state through fluorescence or non-radiative decay due to a forbidden transition. This increases the time scale in which this process occurs from 10^{-19}-10^{-7} s for fluorescence to 10^{-3}-10^{2} s for phosphorescence. These two process can be differentiated through time delayed photoluminescence spectroscopy. Since the excited triplet state is typically lower in energy than the excited singlet state, phosphorescence is red-shifted compared to fluorescence.

1.4 Structure-Property relationship of conjugated polymers

One of the appealing advantages of organic materials used in electronic applications is their structure tunability. The primary structure of a polymer can dictate to a large degree the characteristics that the polymer will have, such as polythiophenes, polyphenlylenes, polypyrroles, etc. Modification of these primary structures is what allows for the tunability of the polymers. Modifications include the addition of donors and acceptors as well as altering the conjugation length.

Conjugation length depends on a number of factors including: 1) the overall length of the polymer 2) the dihedral angle of the conjugated units 3) rigidity of the polymer and 4) the overall 3d structure. An increase in conjugation length corresponds to a decrease in the energy gap between the HOMO and LUMO energy levels. Donor and acceptor groups can increase or decrease the electron density of the conjugated system. Donors are electron rich groups that are conjugated with the rest of the system. This results in the donor group pushing its electrons into the conjugated system resulting in a

higher electron density. As electron density increases, the LUMO energy level of the CP increases. Acceptors are groups that are electron deficient and can be attached to the CP to "pull" electrons off the conjugated system, effectively lowering the electron density of the CP. As electron density is decreased, the LUMO energy level decreases as well. This decrease in energy is due to the decrease in electrostatic repulsion between electrons since less electrons are confined to an area. Figure 1.5 shows some common donor and acceptor moieties.

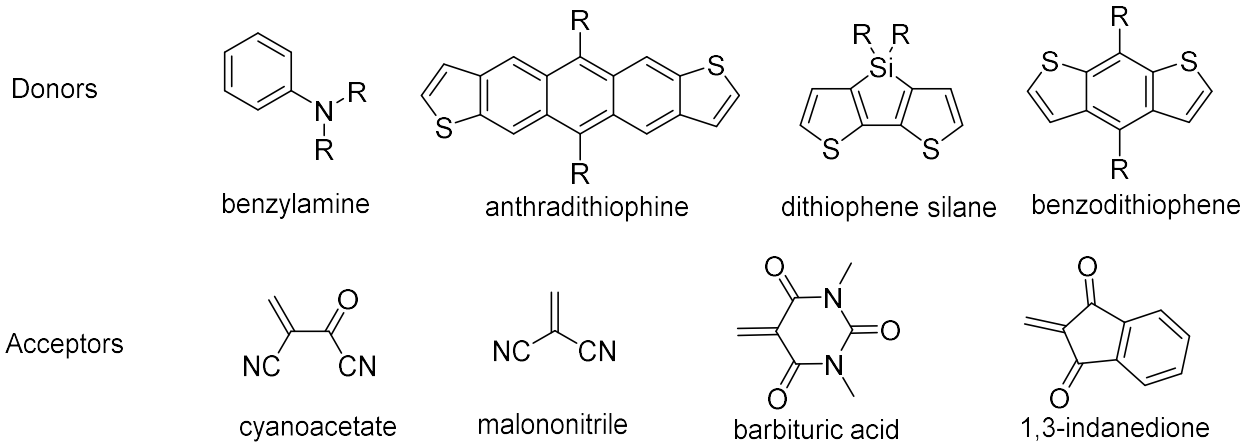

Figure 1.5 Examples of Donors and Acceptors added to conjugated polymers**.**

1.5 Photostability

Photostability of conjugated polymers is the ability of the conjugated backbone of the polymer to stay intact during illumination. Optical density of a CP sample (film or solution) has a positive correlation with the density of conjugated pi bonds. Photodegradation that causes destruction of conjugated pi bonds can be monitored by UV-Vis absorbance. Absorbance measurements are not as affected by the generation of quenching species and morphology changes as photoluminescence measurements are.

Although photoluminescence and absorbance provide information on the extent of photodegradation, they only give a minor amount of information on structural changes

that are occurring in the polymer. In order to study the photodegradation mechanisms in conjugated polymers, it is necessary to determine structural changes occurring in the CPs. Nuclear Magnetic Reasonance (NMR) is an effective tool for the characterization of a wide array of organic compounds. NMR is able to identify protons in a structure and give information on the environment of the protons, (the number and nature of protons of the neighboring protons), and of the number of a particular proton. It is difficult to utilize NMR spectroscopy for photodegradation studies. NMR requires ~ 1 mg of sample to obtain a good spectrum, from which peaks are discernable and relative intensities are measurable. Photodegradation studies typically yield less than 1 mg of degraded products, and trying to identify trace amounts of various compounds in the NMR spectrum isn't possible. Infrared Spectroscopy (IR) identifies functional groups within a compound at a relatively low concentration, and the characteristic peaks of the functional groups appear at fundamental frequencies. Unlike NMR, IR is well suited for analyzing trace amounts of samples. Another advantage to the use of IR, is that it is widely used in photodegradation studies and therefore many of the peaks corresponding to common degradation products have already been identified, eliminating the need to use cumbersome derivatization techniques. We found that IR spectroscopy was the most useful tool for characterizing photodegraded polymer samples. Another tool that is commonly used in photodegradation studies is gas chromatography (GC) or liquid chomatography (LC) with a mass-spectrum (MS) detector. GC/LC MS are great tools for characterization of small organic molecules, but they are less informative when used on macromolecules like polymers.

1.5.1 Reactive oxygen species

The majority of the photodegradation processes occurring in conjugated polymers occur through a process called photo-oxidation, which is initiated by reactive oxygen species (ROSs). Typically, neutral molecules in their ground states do not have unpaired electrons. Dioxygen is a unique molecule in the sense that its lowest energy form is a diradical in a triplet state. This diradical is stable as each oxygen has nine electrons in the valence shell. It requires a large activation energy to undergo a reaction with many organic compounds due to the inversion of spin that is necessary for a reaction to occur. Although dioxygen is stable in its ground state, there are other oxygen species that are much more reactive and are termed ROSs. ROSs play an important role in biology and are natural byproducts of oxygen utilization in organisms. Examples of ROSs include peroxides, hydroxyl radicals, superoxide anion, and singlet oxygen. Peroxides are any compound that contains two oxygen atoms bonded to each other by a single bond. This oxygen-oxygen bond is very unstable and undergoes homolytic bond cleavage to produce oxygen radicals, which then can react with organic compounds to induce oxidation. Peroxides have been observed to form during the photodegradation of some CPs, they often act as intermediates in the radical degradation process.

Superoxide anion is formed through a one electron reduction of molecular oxygen. Superoxide anion plays an important role in Biology, since it is quite toxic, it is utilized by phagocytes to kill pathogens. Superoxide anion can also be produced through the transfer of an electron from the excited state of a conjugated polymer to the LUMO of molecular oxygen. As shown in Figure 1.6, when a CP absorbs a photon of light, an electron is excited to the LUMO of the CP. An Electron in the LUMO can either relax to the HOMO through non-radiative decay or fluorescence. One other option is that, the

electron in the LUMO can be donated to another molecule, in this case oxygen. This transfer of an electron simultaneously produces a superoxide anion and polymer radical cation, which leads to radical degradation of the polymer.

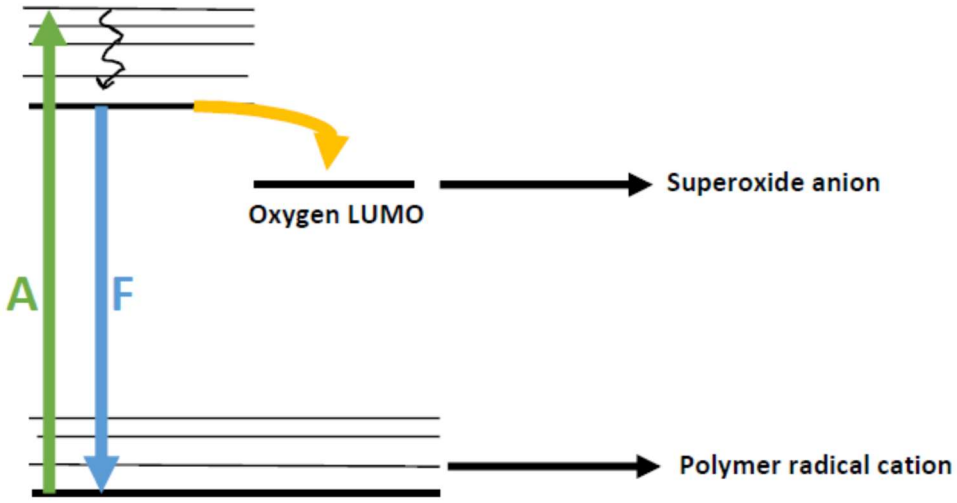

Figure 1.6 Photoinduced one electron reduction of oxygen by a conjugated polymer to produce superoxide anion.

Singlet oxygen, is dioxygen in a high energy state that increases its reactivity towards organic compounds. Triplet state oxygen is unable to react with organic compounds that are in the singlet state, but when triple oxygen is converted into singlet oxygen these reactions are no longer forbidden and take place with ease. Singlet oxygen is produced as a result of an energy transfer between the excited triplet state of a polymer to a molecule of triplet oxygen. When a polymer is excited to the excited singlet state in can relax by one of the processes described earlier or it can undergo intersystem crossing to an excited triplet state. In order for the polymer to relax to its ground state, it can undergo phosphorescence or transfer its energy to another molecule. When it transfers the energy to triplet dioxygen, singlet oxygen is produced. Since singlet oxygen now has the

same multiplicity as typical organic compounds, it becomes much more reactive. The typical reactions that are seen involving singlet oxygen and conjugated polymers are; ene reactions, 2+4 cycloadditions and 2+2 cycloadditions.

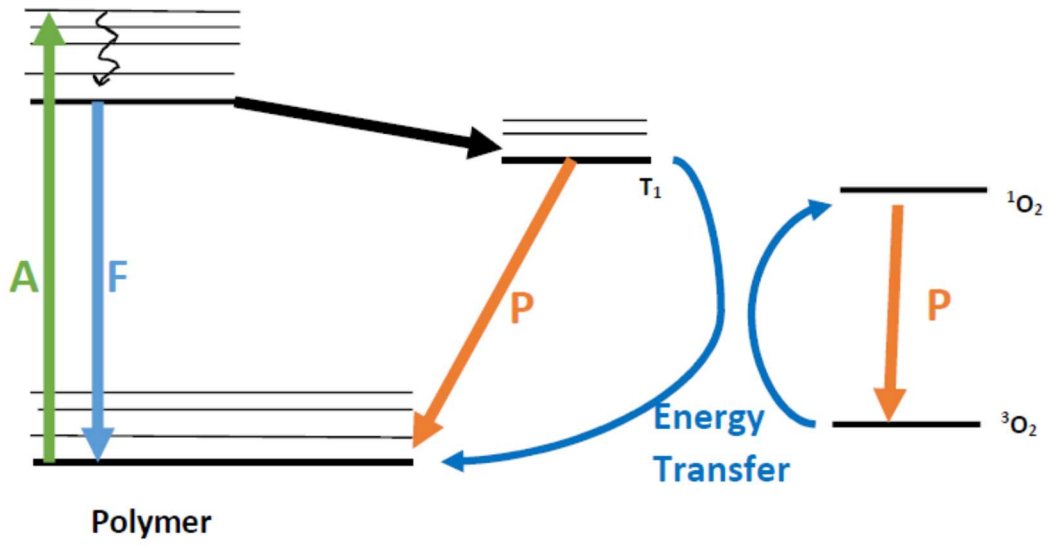

Figure 1.7 Generation of singlet oxygen from the conjugated polymer triplet state

1.5.2 Structure-Photostability Relationship

The photostability of conjugated polymers depends on their chemical and resulting electronic and energy structures, in particular, the LUMO energy level. The LUMO level as discussed previously is determined by the structure of the polymer, including conjugation length and the addition of electron donating and withdrawing groups. One of the primary advantages of using organic materials in electronics applications is the tunability of the LUMO and HOMO energy levels. It has been previously shown that the photostability of many polymers is directly proportional to the LUMO energy level, the higher the LUMO energy level, the less photostable the polymer.[24] This is due to the electronic processes that occur when the polymer is in the excited singlet state. The polymer can undergo any of the optical processes outlined

earlier, or it can donate an electron to a molecule or polymer with, either, a lower LUMO level or a hole in the HOMO level. When the LUMO level is increased, it increases the likelihood that an electron will possess enough energy to be donated to another molecule. When this electron transfer occurs, radical degradation is initiated. Radical degradation typically occurs much faster than singlet oxygen degradation. This is why we see a strong correlation between the LUMO energy level of a CP and the rate of photodegradation. Beyond the LUMO level, side chains and non-aromatic double bonds have been shown to increase the rate of photodegradation. When radical degradation is initiated it typically occurs on the side-chain of a CP through hydrogen abstraction. Previous research has shown that removal of the side chains increases the photostability of the polymer.[25] When a CP photodegrades through a singlet oxygen mechanism, side-chains and the LUMO energy level contribute very little to the rate of photodegradation. During singlet oxygen induced degradation, the main factor determining the rate of degradation is the efficiency of intersystem crossing. The most susceptible place for a CP to be attacked by singlet oxygen is at non-aromatic double bonds. Double bonds can readily undergo cycloadditions with singlet oxygen. On the other hand, the rate of cycloaddition of singlet oxygen to aromatic rings is much lower, due to the energy required to break aromaticity.

1.6 Research Objective

This investigation aims to gain a better understanding of the structure-photostability relationship of conjugated polymers. This goal will be achieved through a study of the photodegradation mechanisms of various conjugated polymers. The study is initiated by comparing two dicyano-substituted polyphenylenevinylenes (PPVs). PPVs are commonly used in OLEDs and PSCs. Due to their wide spread use, the photostability

of PPVs has been thoroughly investigated. It was previously discovered that the addition of cyano substituents on the backbone of PPV lowered its LUMO energy level, while increasing its photostability.[26] To expand on that study, the effects that different side chains have on PPV photostability was investigated, these results are discussed in Chapter 2. Little research has focused on how the characteristics of side chains, effect the device performance and photostability. Side chains are typically only an afterthought of the molecular design process, to ensure processability of the polymer. In this study, it was observed that the nature of the side chain can have a large impact on various polymer properties such as; absorbance, fluorescence, HOMO/LUMO energy levels and photostability.

There are many strategies to increase the photostability of CPs, including; lowering the LUMO level, encapsulation, removal of side chains, fluorination and addition of antioxidants. Antioxidants work in one of two ways, either through radical quenching or triplet state quenching. It is common for radical quenchers to be added to polymers to slow their degradation due to UV light. For polymers that degrade by singlet oxygen, a triplet state quencher or a singlet oxygen quencher may be used to reduce the rate of photodegradation. In Chapter 3, addition of a known singlet oxygen quencher and its effect on the photodegradation of RO-diCN-PPV and C8-diCN-PPV is investigated.

Photostability is a major issue in PSCs, the longest t_{80} to date is 3.4 years. In other words, the most photostable PSC takes 3.4 years, of exposure to 1 sun, to degrade to 80% of its original power conversion efficiency.[27] A large amount of research has focused on increasing the PCE of PSCs in order to make them more cost competitive with their inorganic counterparts. Another approach to reducing the cost ($/kWh) of PSCs, is to

increase their operational lifetime. In Chapter 4, P3HT, a polymer that has been studied extensively for PSC applications, is compared to a newly synthesized polymer that shares structural similarities w/ P3HT.

Chapter 2 Photochemical Stability of diCyano-Substituted Poly(Phenylenevinylenes) with Different Side Chains

2.1 INTRODUCTION

Conjugated polymers (CPs) are a subject of intense research for their application in organic photovoltaics (OPVs),[1-2] organic light emitting diodes (OLEDs),[5-7] solid-state dye lasing,[8-9] biological imaging and sensing,[10-14] chemical sensing[15-18] and remote sensing. One of the main hurdles to widespread application of CPs in these applications is their susceptibility to photodegradation, which causes loss of mechanical properties and most importantly changes in their photophysical characteristics. Photodegradation in conjugated polymers has been intensively studied in poly(3-hexylthiophene) (P3HT) and poly(phenylenevinylene) (PPV).[28-29] There has been debate over the mechanism responsible for photodegradation in these polymers. The consensus for P3HT and PPV is a radical degradation mechanism.[30-32] When illuminated in the presence of oxygen, the polymer donates an electron through charge transfer to oxygen forming a polymer cation and superoxide radical anion. In the case of PPVs, the superoxide radical anion can react with a side chain abstracting a hydrogen, forming a carbon radical. It can also attack a vinylene unit in the backbone, producing a peroxide anion and a carbon radical.[31] Hoke et al. and Dam et al. have shown that the LUMO (lowest unoccupied molecular orbital) energy level of a polymer is directly related to the rate of photodegradation.[24, 33] This holds true with respect to the polymers that are known to degrade by a radical mechanism. Poly(2,5-bis(decyloxy)-1,4-phenylenevinylene) (RO-PPV) with a LUMO level of –2.91 eV degrades faster than poly(2,5-bis(decyloxy)cyanoterephthalylidene) (CN-PPV) with a LUMO level of –3.29 eV.[26] To increase the stability of PPV-type

polymers we synthesized a poly(2,5-bis(decyloxy)-1,4-phenylene-1,2-dicyanovinylene) (RO-diCN-PPV), the dicyano substituents on the vinylene unit lowered the LUMO level from –2.91 eV for RO-PPV to –3.54 eV. RO-diCN-PPV shows a greater photostability than RO-PPV, which is in line with the observation of Hoke et al. and Dam et al. A poly(2,5-dioctyl-1,4-phenylene-1,2-dicyanovinylene) (C8-diCN-PPV) polymer, first synthesized by Moslin et. al.,[34] shows faster photodegradation than RO-diCN-PPV despite having a lower LUMO energy level (–3.69 eV). The deviation from this common understanding about the structure-photostability relationship is investigated. The mechanisms for dicyano-substituted poly(phenylenevinylenes) (diCN-PPVs) are elucidated using infrared (IR) and photoluminescence (PL) spectroscopy and PL quenching experiments. It was concluded that singlet oxygen is responsible for the higher rate of photodegradation observed for C8-diCN-PPV due to intersystem crossing to its triplet state. Formation of an imide linkage, a side reaction of dicyanovinylene formation which was unnoted in the previously reported synthesis of RO-diCN-PPV[26] and C8-diCN-PPV[34] was identified, and the synthesis of these polymers was modified to avoid this structural defect from the side reaction.

2.2 EXPERIMENTAL

NMR data were obtained from a Bruker Avance 400 MHz NMR Spectrometer, and a Bruker Avance 600 MHz NMR Spectrometer as specified. Molecular weights of polymers were determined using an Agilent 1100 series HPLC system, equipped with two GPC columns (PL1110-6500, PLGel 5 mm MIXED-C 7.5×300 mm). Polystyrenes were used as the standards for conventional calibration and tetrahydrofuran was used as the solvent. The polymer films were spin-coated from the polymer solutions in *o*-

dichlorobenzene on glass substrates. The optical density of the films was kept between 0.2 and 0.3, except when indicated. UV-vis spectra were obtained from an Agilent 8453 photodiode array UV-vis absorption spectrophotometer.

Photoluminescence (PL) was measured on a Perkin Elmer LS-50B luminescence spectrometer. All measurements were performed in air with no inert gas purging to protect film or solutions except where indicated. Measurements performed under nitrogen where carried out on a small glass slide affixed inside a quartz cuvette, which was sealed inside a nitrogen filled glovebox. The emission correction was performed in the range of 200-900 nm using deuterium-tungsten light source with known spectral distribution. A high power Newport light source (model 66903) equipped with a 300 W xenon arc lamp and a Newport power supply (Model 69911) was used for the photostability study. The output from the light source was used without filtering. Light Intensity was adjusted through a focus lens and measured by a Newport 70260 power meter with a 3A-P-SH – V1 thermal head. The aperture diameter of the power meter is 1.2 cm and the unit intensity is calculated to be 2200-2600 mM/cm^2, 22-26 times that of one standard sun intensity.

Infrared spectra were measured on a Thermo Scientific Nicolet iS5 FT-IR spectrometer with ZnSe Windows. The samples were drop coated on a KBr plate in ambient air. The samples were photodegraded on the KBr plate and IR analysis was done immediately after illumination.

Cyclic voltammetry (CV) measurements were performed on the polymer films coated on a Pt working electrode in a tetrabutylammonium hexafluorophosphate (0.1 M)/acetonitrile solution with a silver/silver nitrate reference electrode. The redox couple

ferrocene/ferricenium ion (Fc/Fc^+) was used as an external reference. The HOMO and LUMO levels were calculated using the $E_{ox,onset}/E_{red,\ onset}$ and are summarized in Table 2.1. The calculations were done using the relation $E^{\text{HOMO/LUMO}} = \left[E_{\text{onset(vs.Ag/AgCl)}} - E_{(\text{Fc/}Fc^{+}\text{vs. Ag/AgCl})}\right] - 4.8\ eV$.[35] The band gap was determined by the difference between the LUMO and HOMO.

2,5-Bis(bromomethyl)-1,4-bis(octyl)benzene (2). A solution of 1,4-dioctylbenzene (**1**) (3.93 g, 13 mmol), paraformaldehyde (1.56 g, 52 mmol), tetrabutylammonium bromide (0.2 g), and 33% hydrobromic acid in acetic acid (25 mL) was heated at 110 ºC for 96 hours. The reaction was then cooled to RT and water (20 mL) was added. The precipitate was formed and collected via filtration. The solid was then dissolved in hexane and filtered through a silica gel plug using hexanes as the solvent. The filtrate was then recrystallized from hexanes producing a white solid. Yield: 50%. ^{1}H NMR ($CDCl_3$) of **2**: δ (ppm) 0.89 (t, J=6.38 Hz, 6H), 1.25-1.45 (m, 20H), 1.63 (quint, J=7.55, 4H), 2.66 (t, J=9.06 Hz, 4H), 4.49 (s, 4H), 7.14 (s, 2H). The spectrum is consistent with that of 2,5-bis(bromomethyl)-1,4-bis(hexyl)benzene found in literature.[36]

2,5-Bis(cyanomethyl)-1,4-bis(octyl)benzene (3). Synthesized following the procedure reported by Moslin et al.[34]

Poly(2,5-dioctyl-1,4-phenylene-1,2-dicyanovinylene) (C8-diCN-PPV). To compound **3** (200 mg, 0.52 mmol) in dry THF (3 mL) at RT under a nitrogen atmosphere was added freshly prepared lithium tetramethylpiperidide (359 mg, 2.1 mmol) in a mL of dry THF. Next, iodine (0.41 g, 1.62 mmol) in dry THF was added. The solution was stirred for 20 minutes. The mixture was poured into 20 mL of methanol while stirring. The solid was filtered giving a dark orange solid with a yield of 140 mg (70 %) ^{1}H NMR ($CDCl_3$) of

C8-diCN-PPV: δ (ppm) 0.89 (bs, 6H), 1.29 (bm, 20 H), 1.5-1.8 (bm, 4), 2.25-2.91 (bm, 4H), 6.57-6.90 (bm, 1H), 7.18-7.47 (bm, 1H).

Poly(2,5-di(decyloxy)-1,4-phenylene-1,2-dicyanovinylene) (RO-diCN-PPV). Synthesis of **RO-diCN-PPV** from **4** (200 mg, 0.32 mmol) used the same procedure as the synthesis of **C8-diCN-PPV** except for using 3 molar equivalents of lithium tetramethylpiperidide (188 mg, 1.28 mmol) and no addition of iodine. Yielded 133 mg (91 %) of an orange solid. ^{1}H-NMR ($CDCl_3$) of **RO-diCN-PPV**: δ (ppm) 0.86 (bs, 12H), 1.2-1.6 (bm, 56 H), 1.75-1.9 (bm, 8H), 3.6-4.2 (bm, 4H), 6.55-6.80 (bm, 1H), 7.05-7.25 (bm, 1H).

2.3 RESULTS AND DISCUSSION

2.3.1 Synthesis.

The synthesis of **2** used a procedure similar to that used by Brehm et al. for the synthesis of 1,4-dihexyl-2,5-bis(bromomethyl)benzene.[36] Initially, following this procedure yielded very little product, due to the formation of a biphasic solution. A phase transfer catalyst (tetrabutylammonium bromide) was added, resulting in a 50% yield after 4 days of reaction. Compound **3** was prepared as previously reported by Moslin et al.[34] In the polymerization step, the C8-diCN-PPV literature procedure was initially followed.[34] The IR spectra (Figure 2.1) of the polymer after acidic workup (as used by Moslin et al.)[34] showed an imide from a known reaction (Scheme 2.2).[37] When the polymers were worked up by a direct precipitation of the basic reaction mixture in MeOH (as was done in our previous synthesis of RO-diCN-PPV),[26] the intermediate did not have a chance to be hydrolyzed into the imide, as a result, an imide peak (1710 cm^{-1}) is not seen in the IR spectrum (Figure 2.1). Since the side reaction was initiated by the

attack of *t*-BuOK as a nucleophile, a bulkier base, lithium tetramethylpiperidide (LiTMP), was used in the polymerization reactions for both RO-diCN-PPV and C8-diCN-PPV (Scheme 2.1). The ^{1}H NMR spectra of the two polymers (Figures 2.2 and 2.3) show that *trans* C=C is dominant. The IR spectra (shown in the photostability section) show that the side reaction was completely avoided. The yield for the synthesis of C8-diCN-PPV from compound **1** was 26%.

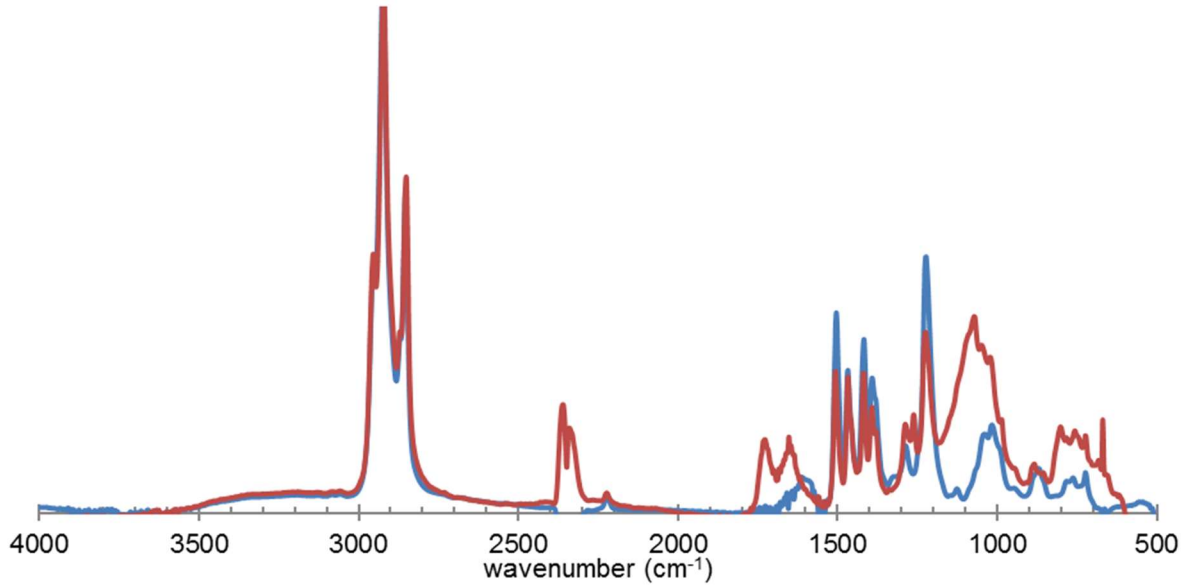

Figure 2.1 The IR spectra of RO-diCN-PPV worked up in MeOH (blue) and worked up with dilute HCl (red). When the polymers were worked up by a direct precipitation of the basic reaction mixture in MeOH, the intermediate did not have a chance to be hydrolyzed into the imide, as a result, an imide peak (1710 cm^{-1}) is not seen in the IR (blue)

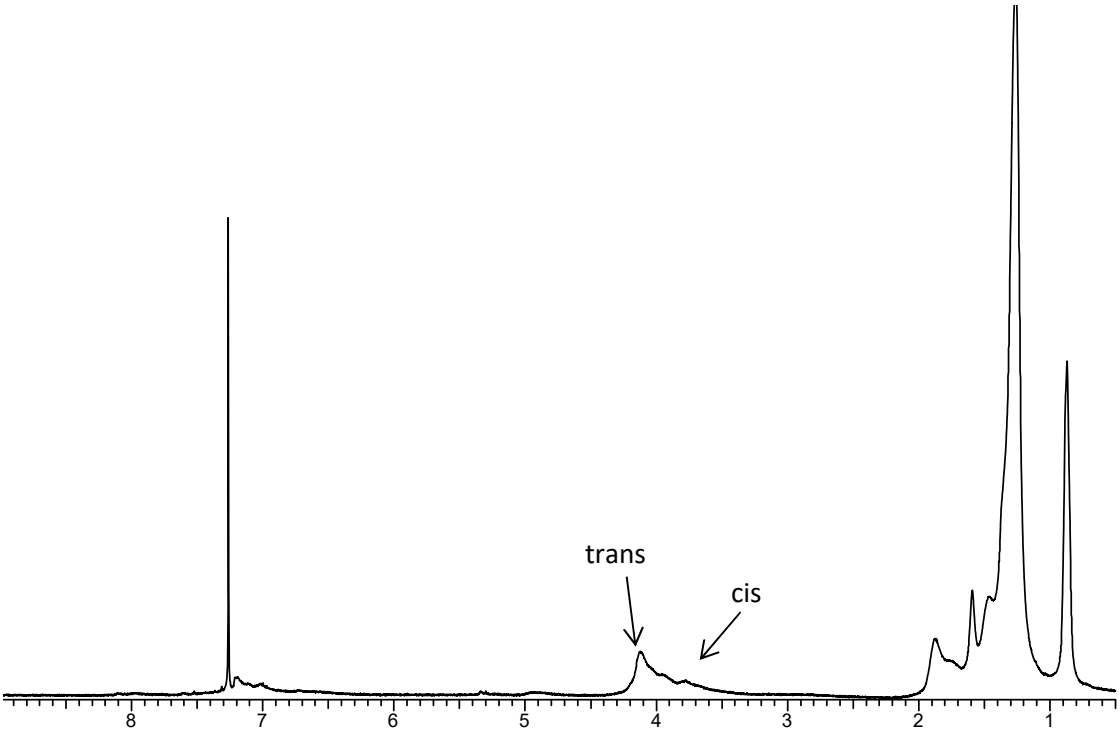

Figure 2.2 ^{1}H-NMR spectrum of RO-diCN-PPV in CDCl3

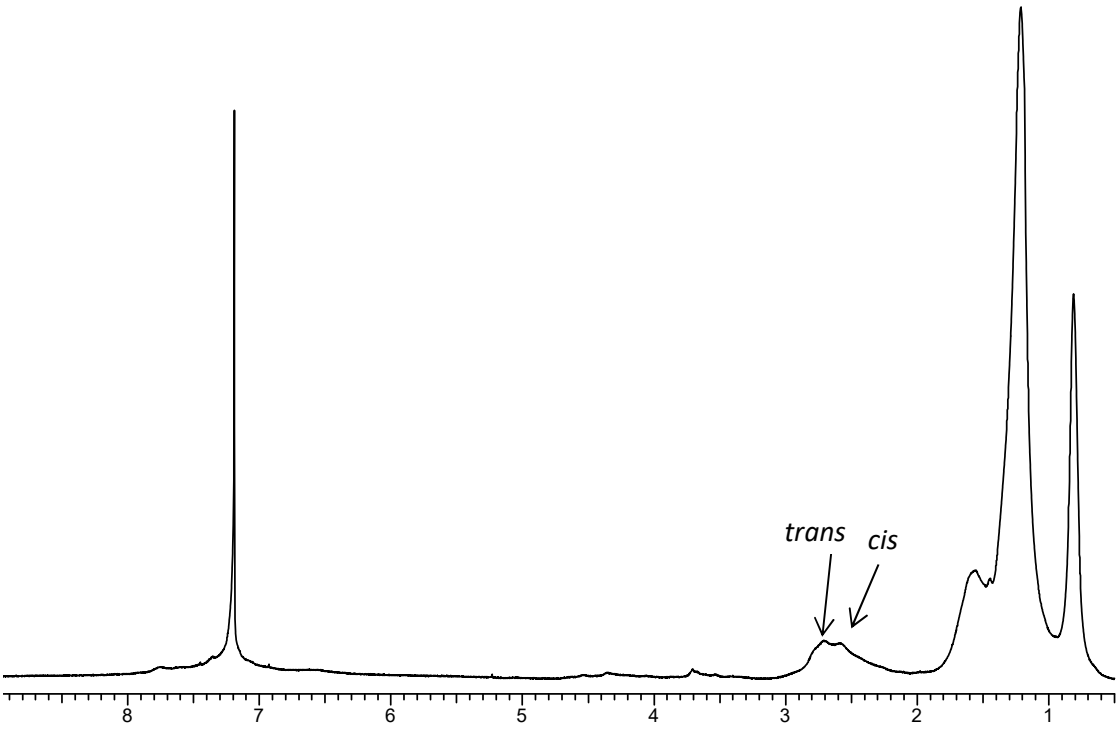

Figure 2.3 ^{1}H-NMR spectrum of C8-diCN-PPV in CDCl3

Scheme 2.1 Synthesis of C8-diCN-PPV and improved polymerization reaction for RO-diCN-PPV. The monomers **3**[34] and **4**[26] were previously reported.

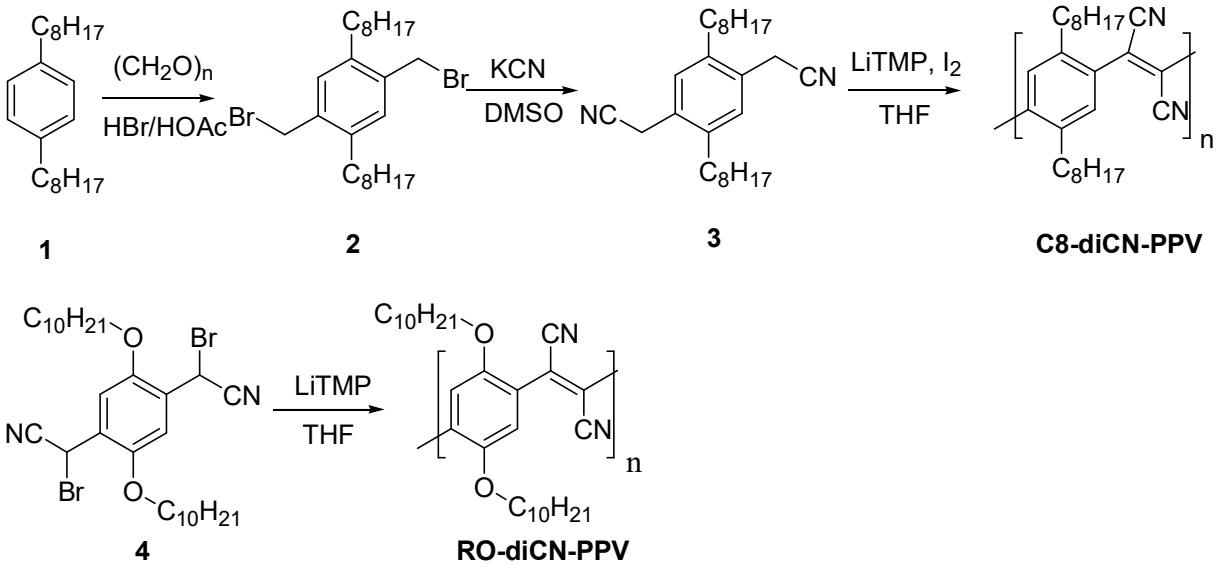

Scheme 2.2 Formation of imide when t-BuOK was used as the base in the polymerization reaction. Dilute acid is necessary to hydrolyze the intermendiate **B** into the imide **C**.

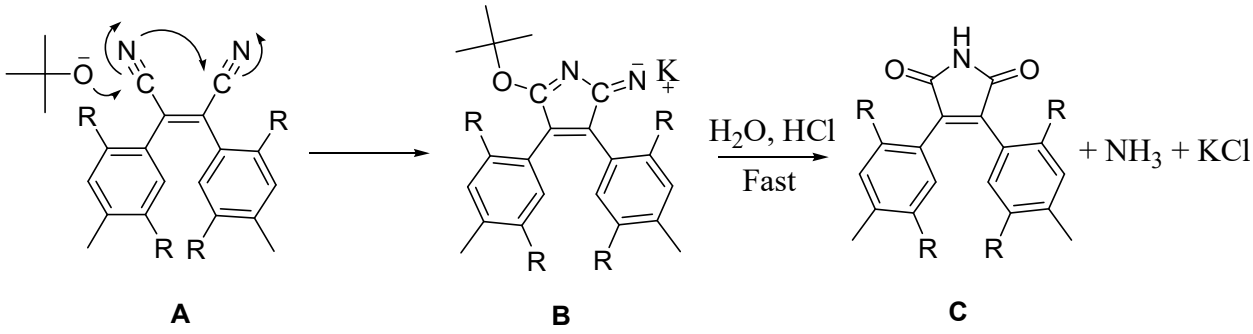

2.3.2 Optical Absorption, physical and Electrochemical Properties

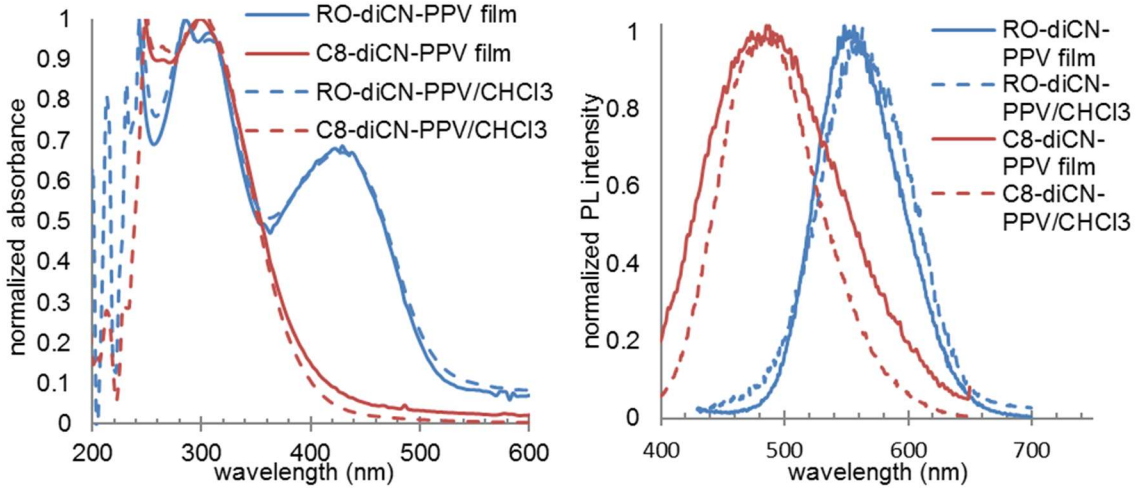

Figure 2.4 Left: UV-Vis absorbance spectra of the polymers in film and solution. Right: Photoluminesence spectra of the polymers in film and solution; excitation wavelengths: 385 nm for C8-diCN-PPV and 400 nm for RO-diCN-PPV.

The absorption spectra of RO-diCN-PPV and C8-diCN-PPV are shown in Figure 2.4. The band gap as estimated from the absorption spectra for C8-diCN-PPV is 0.67 eV greater than that of RO-diCN-PPV, most likely due to the lack of a donor-acceptor interaction in C8-diCN-PPV. The cyclic voltammogram of RO-diCN-PPV, C8-diCN-PPV and Air is shown in Figure 5 and the results of the energy level calculations are summarized in Table 2.1. No oxidation peak was observed for C8-diCN-PPV. Over-potential in the CV measurement often gives a higher bandgap than observed for the optical bandgap,[26] which is the case with RO-diCN-PPV. The lower LUMO level of C8-diCN-PPV is a result of the lower electron donating ability of the alkyl side chains as opposed to the alkoxy side chains. The molecular weight of the polymers was measured using GPC and the results are summarized in Table 2.1.

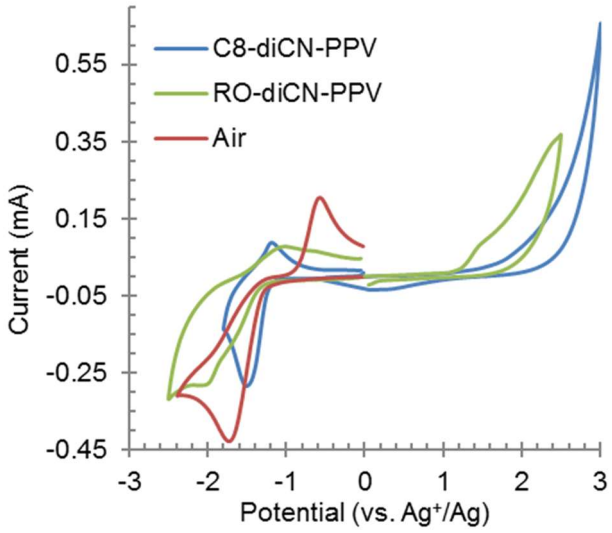

Figure 2.5 Cyclic voltammograms of C8-diCN-PPV, RO-diCN-PPV and Air.

Table 2.2 Optical and electrochemical characterization results of the RO-diCN-PPV[26] and C8-diCN-PPV.

	M_w/M_n (kDa)	λ^{abs}_{max}/nm (eV) sol./film	E_g^{opt}/eV sol./film	λ^{PL}_{max}/nm sol./film	LUMO/HOMO/E_g (eV)
RO-diCN-PPV	14/7.4	440/440 (2.82/2.82)	2.32/2.38	564/555	-3.54/-6.04/3.50
C8-diCN-PPV	8.2/4.5	295/293 (4.20/4.23)	2.99/2.82	491/486	-3.69/--/--

2.3.3 Photoluminescence (PL) Study

PL spectra of RO-diCN-PPV and C8-diCN-PPV are shown in Figure 4. The thin film PL peak wavelengths are 484 and 555 nm for C8-diCN-PPV and RO-diCN-PPV respectively. The PL λ_{max} for C8-diCN-PPV is slightly longer by 5 nm than previously reported by Moslin et al.[34] which is due to the higher content of *trans* C=C in the newly

synthesized polymer compared to the polymer synthesized by Moslin et al. The PL λ_{max} for C8-diCN-PPV is blue shifted by 71 nm compared to RO-diCN-PPV.

2.3.4 Photostability

The photostability of the polymers were studied using a xenon arc lamp. The beam was focused to give an intensity 22-26 times that of one standard sun. This was used to accelerate the photooxidation of the polymers. The photooxidation of the polymers was monitored using UV-vis absorbance, as this measurement is not affected by quenching impurities like photoluminescence measurements are. The initial photoxidation rate of C8-diCN-PPV is 7 times greater that of RO-diCN-PPV (Figures 2.6 & 2.7). The faster photodegradation of the alkyl substituted diCN-PPV polymer compared to the alkoxy substituted polymer was first shown by Moslin et al.[34] in comparing C8-diCN-PPV with MDMO-diCN-PPV.

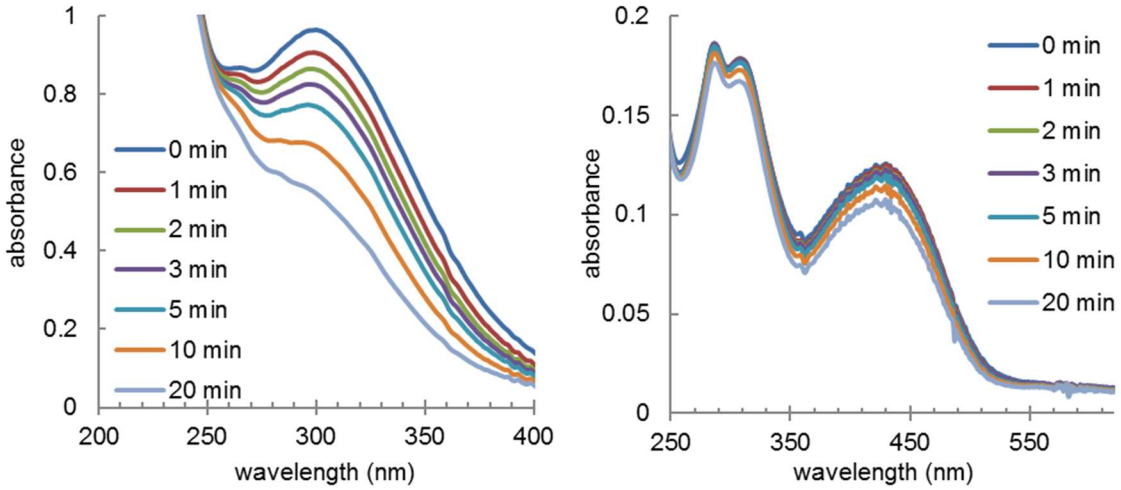

Figure 2.6 Evolution of UV-vis spectra of C8-diCN-PPV (Top) and RO-diCN-PPV (Bottom) with increasing accumulated illumination time.

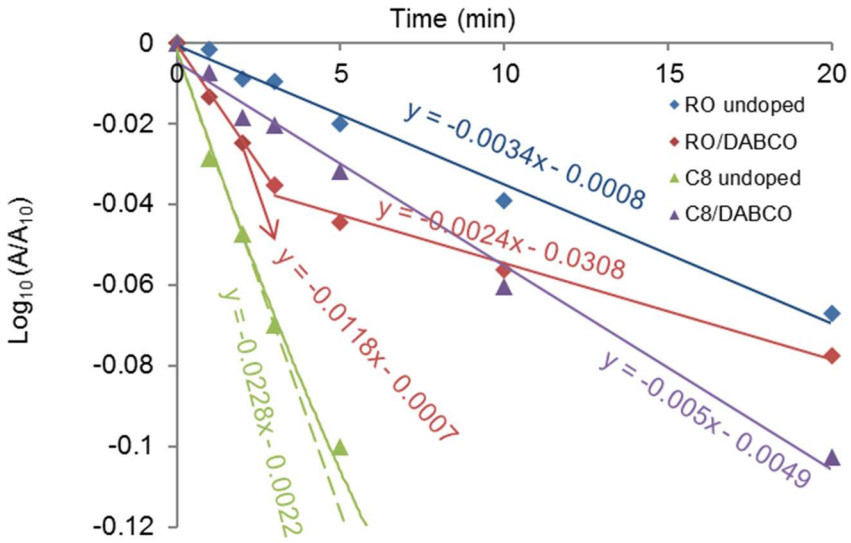

Figure 2.7 Photodegradation of films of RO-diCN-PPV and C8-diCN-PPV, and films of these two polymers doped with 15 wt% DABCO, shown as semilog plots of peak absorbance vs. total accumulated illumination time. The initial peak absorbances were normalized. DABCO doping experiments are discussed in a later section-Degradation Mechanism

2.3.5 Characterization of Photodegradation Products

In the IR absorption spectra of C8-diCN-PPV (Figure 2.8), two new peaks at 1720 cm^{-1} and 3350 cm^{-1} (broad) arise with illumination, and are assigned to C=O in a carboxylic acid,[38] and O–H, respectively. The plots of the intensities of the two peaks as functions of illumination time (Figure 2.9) show similar rates of growth for the two peaks, suggesting that the broad OH at 3350 cm^{-1} is from a carboxylic acid, rather than a phenol. This is further supported by the observation that *p*-methoxyphenol gives a sharper O–H stretching peak than that of *p*-methoxybenzoic acid (Figure 2.10, both doped in RO-diCN-PPV). The integration of the C–H stretching peaks at 2852 and 2925 cm^{-1} (over a range of 2350 and 3100 cm^{-1}) remains constant between 0 min and 240 min

of illumination (with a difference of only 0.25%), indicating almost no decomposition of the alkyl side chain. The apparent drop in the heights of the two peaks is due to broadening of the peak as the polymer is degraded.

A shoulder peak in Figure 8 at the high wavenumber side of the 1720 cm^{-1} peak is due to the carbonyl bond in oxo-acetonitrile (-C(O)CN) as indicated by the similarity to carbonyl stretching in phenyl-oxo-acetonitrile.[39] The formation of the oxo-acetonitrile group can also be monitored by the disappearance of the nitrile stretching peak at 2227 cm^{-1} and the appearance of a new nitrile stretching peak at a higher wavenumber 2258 cm^{-1} which is consistent with the nitrile stretching of a phenyl-oxo-acetonitrile.[39] This group is not stable to moisture and the CN peak can be completely lost if the photodegraded polymer is transferred from a glass slide onto a KBr plate using a solvent (e.g., dichloromethane), a procedure used in the early stage of this study. The acyl cyanide is known to undergo hydrolysis in the presence of moisture to form the corresponding carboxylic acid.[40]

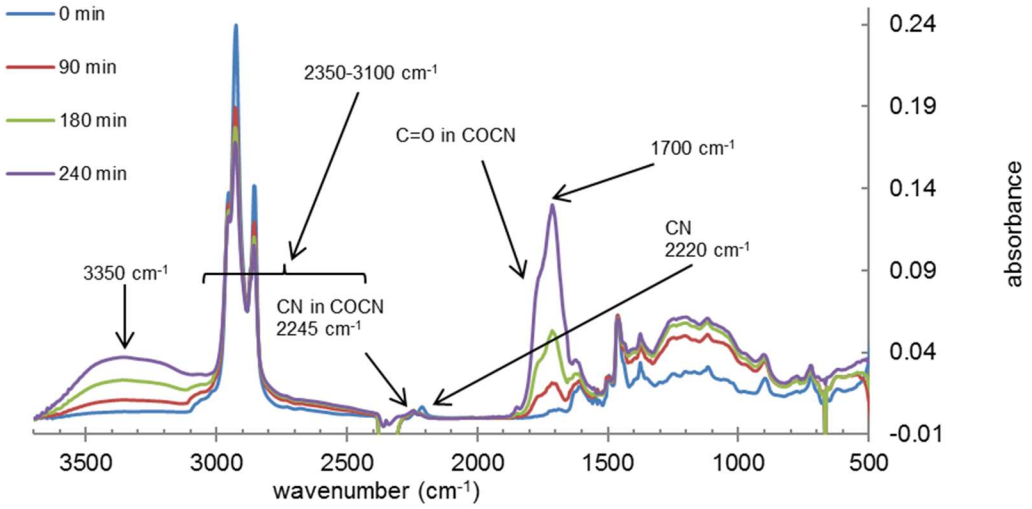

Figure 2.8 Infra-red absorption spectra of C8-diCN-PPV as a function of total illumination time**.**

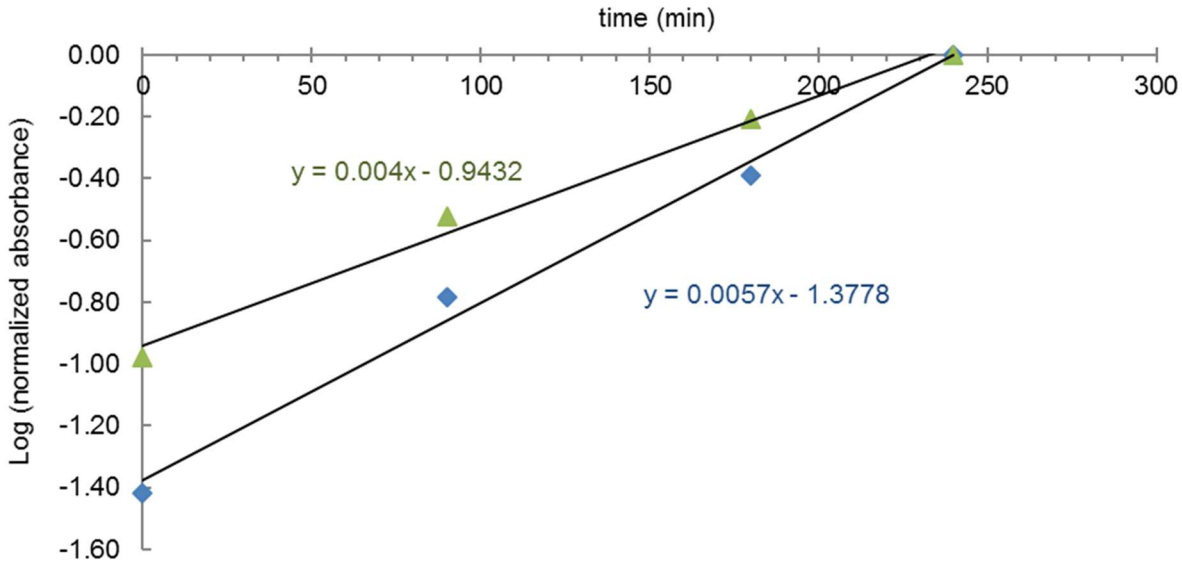

Figure 2.9 Plot of the C8-diCN-PPV carbonyl peak height at 1709 cm^{-1} (blue) and the OH peak height at 3370 cm^{-1} (green) versus (accumulated) film illumination time.

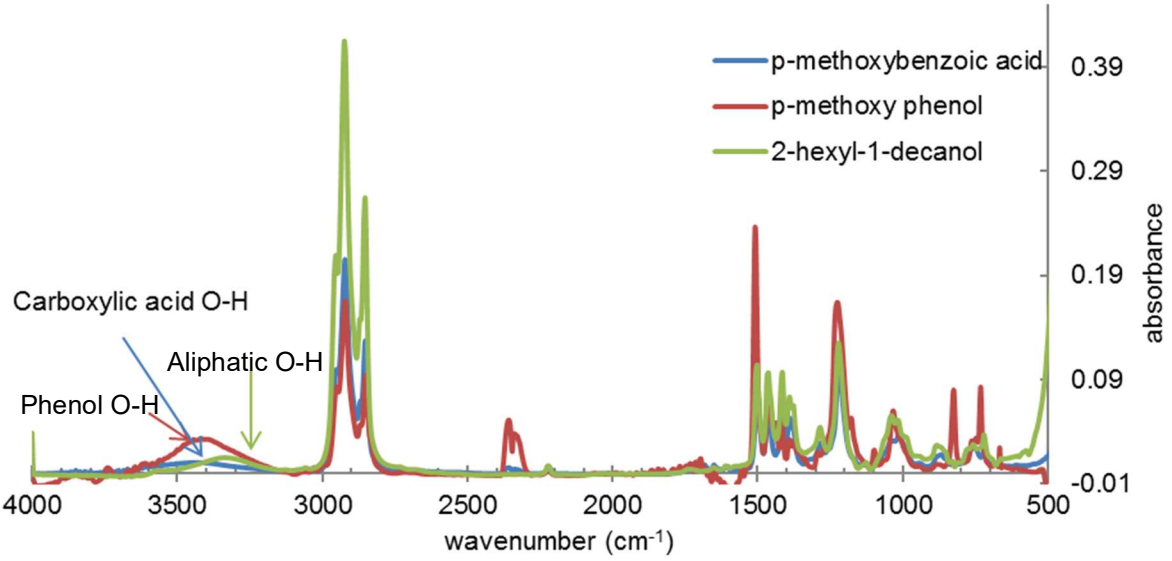

Figure 2.10 IR spectra of RO-diCN-PPV with 15% p-methoxybenzoic acid (blue), 15% p-methoxy phenol (red), and 15% of 2-hexyl-1-decanol (green).

The photodegradation of RO-diCN-PPV yields similar carbonyl and OH IR peaks to those of C8-diCN-PPV but appearing at wavenumbers 30 cm^{-1} higher. During the course of illumination between 0 and 180 min the integration of alkyl chain C-H peaks at 2850 and 2920 cm^{-1} remains unchanged. The similarity between the photodegradation products of both polymers suggests a similar degradation mechanism. From the ratio of OH and CH peak integrations, the degradation rate ratio of C8-diCN-PPV to RO-diCN-PPV over the 180 minutes of illumination time was estimated to be 4.59.

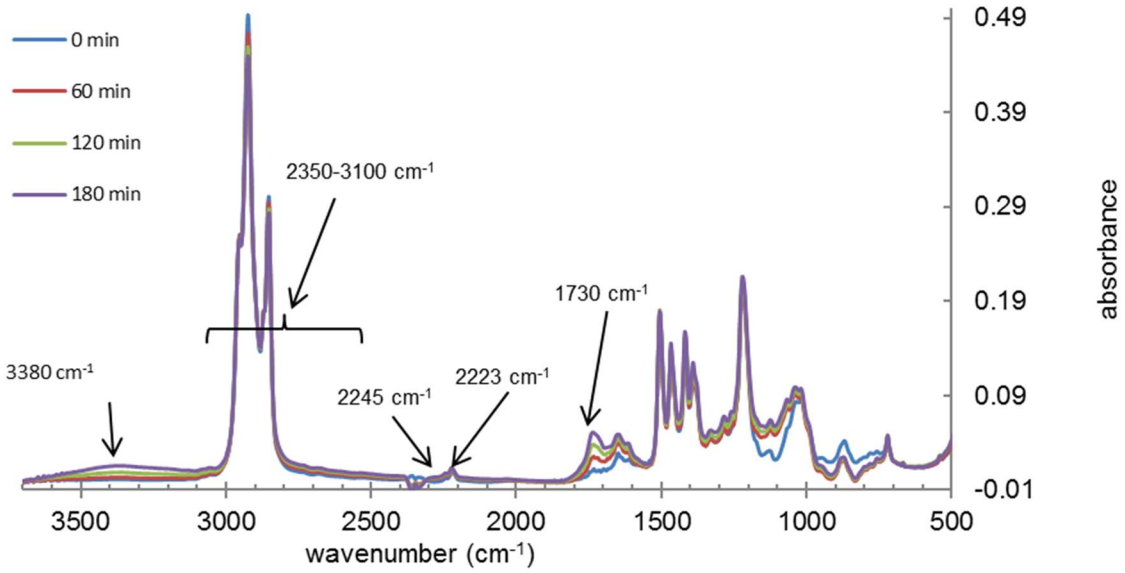

Figure 2.11 Infra-red Absorbance spectra of RO-diCN-PPV as a function of total illuminated time.

2.3.6 Degradation Mechanism

Previous literature has indicated that the main photodegradation mechanism in PPV type polymers involves O_2 radical anions.[24, 30-31] This would occur more rapidly with a polymer that has a higher LUMO level as reported by Hoke et al.[24] We have previously showed that the addition of cyano groups lowers the LUMO level of alkoxy PPV polymers, and the lowering of the LUMO level increased the photostability of the

polymers.[26] This fails to explain the relative photostability of C8-diCN-PPV and RO-diCN-PPV. The LUMO level of C8-diCN-PPV is lower than that of RO-diCN-PPV, yet the initial degradation rate is 7 times greater. Our IR analysis of the degradation products for both diCN-PPVs shows that the main decomposition product is a carboxylic acid formed from the vinylene units in the backbone. This suggests that singlet oxygen is the main culprit in C8-diCN-PPV and RO-diCNPPV, as it would only attack the vinylene units.[33, 41] Radical superoxide anions can be ruled out as they would attack the side chain of the polymer in addition to the vinylene units.

During PL measurements of C8-diCN-PPV a shoulder was noted at 520-530 nm that was highly dependent on film processing. Figure 2.12 shows how strong the shoulder can be. The shoulder is most likely from phosphorescence of the polymer. To confirm this, a C8-diCN-PPV film sample, spin-coated from a 4:1 chloroform and dichlorobenzene solution, was placed inside a quartz cuvette which was sealed in a N_2 glovebox so that the film could be measured in nitrogen or air (after the seal was removed). The intensity of the shoulder peak (Figure 2.13) is stronger in nitrogen than in air. A time-delayed luminescence measurement was conducted in nitrogen with a delay time of 2 ms and an integration gate time of 1 ms. A different PL spectrum was obtained as shown in Figure 2.13. Only one peak is seen at the wavelength of the shoulder peak, confirming the phosphorescence nature of the shoulder peak. We also recorded PL spectra after different delay times (Figure 2.14) and calculated the phosphorescence lifetime for C8-diCN-PPV in air (2.4 ms) and in nitrogen (4.2 ms) (Figure 2.15). The shorter phosphorescence lifetime in air is due to triplet quenching by oxygen. Oxygen quenches the triplet state of the polymer through an energy transfer resulting in in the

formation of singlet oxygen.[42] No phosphorescence was detected for RO-diCN-PPV on our instrument, indicating a much slower intersystem crossing in RO-diCN-PPV.

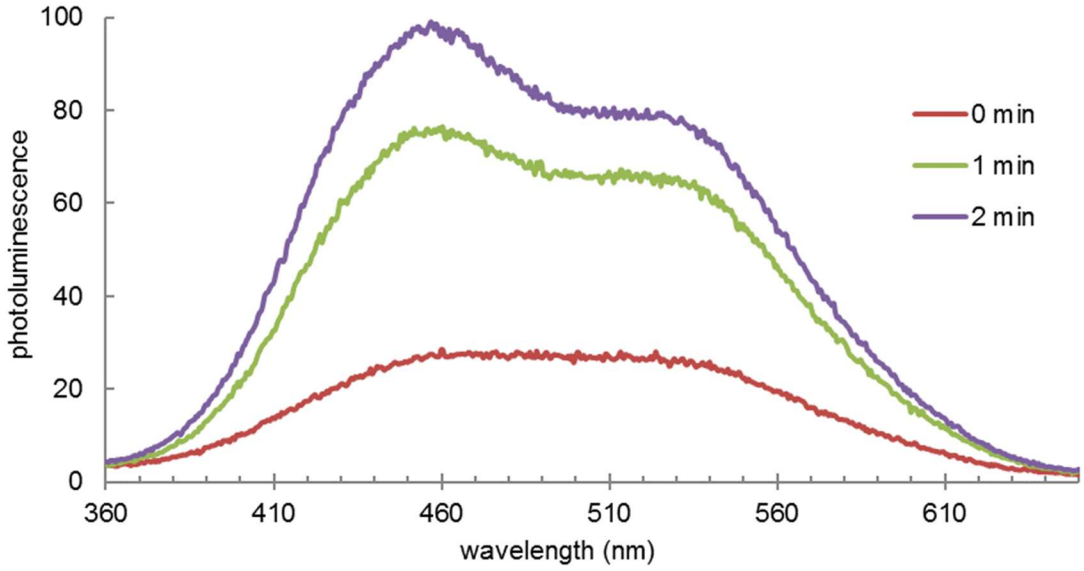

Figure 2.12 PL spectra of C8-diCN-PPV after 0, 1, and 2 minutes of illumination, showing a strong shoulder peak.

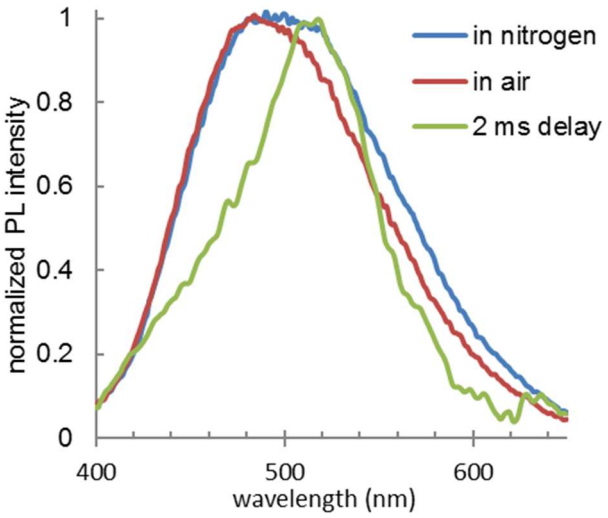

Figure 2.13 PL spectra of C8-diCN-PPV recorded in nitrogen, air, and in nitrogen 2 ms after

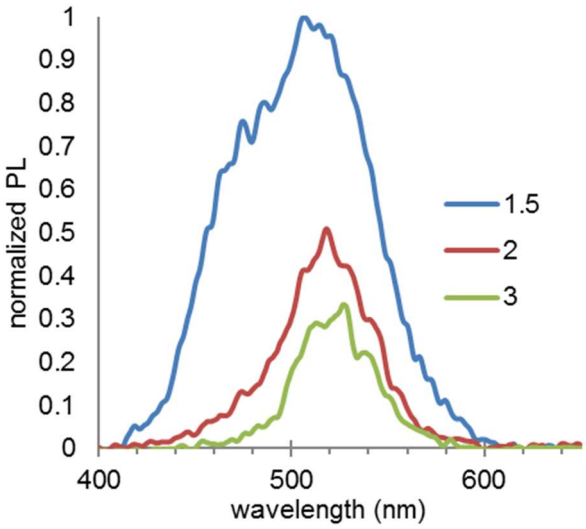

Figure 2.14 Photoluminescence spectra of C8-diCN-PPV in nitrogen at 1.5, 2, and 3 milliseconds after excitation.

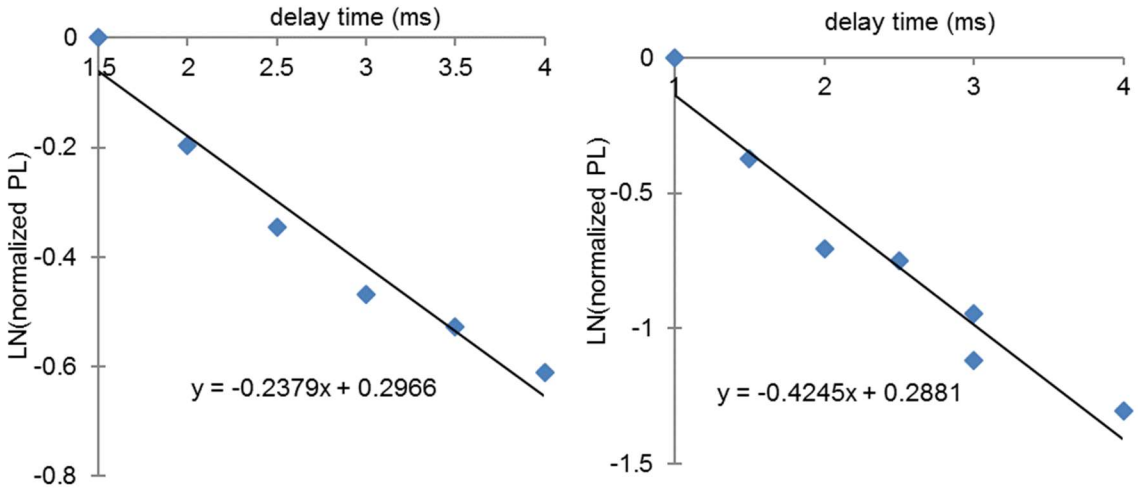

Figure 2.15 Phosphorescence lifetime in nitrogen = 4.2ms (Left) in air = 2.4ms (Right)

We also examined the effect of 1,4-diazabicyclo[2.2.2]octane (DABCO), a known triplet state quencher,[43] on photodegradation of the two polymers. UV-vis spectra of 15 wt.% DABCO-doped polymers with increasing (accumulated) illumination time are shown in Figure 2.16, and the semilog plots of the normalized peak absorbance versus

illumination time are shown in Figure 2.7. With DABCO doping, degradation rate of C8-diCN-PPV film decreased by ~65%, confirming that the triplet state of C8-diCN-PPV plays a key role in the rate of degradation. IR spectra of DABCO-doped C8-diCN-PPV (Figure 2.17) shows that the DABCO was not consumed during the illumination.

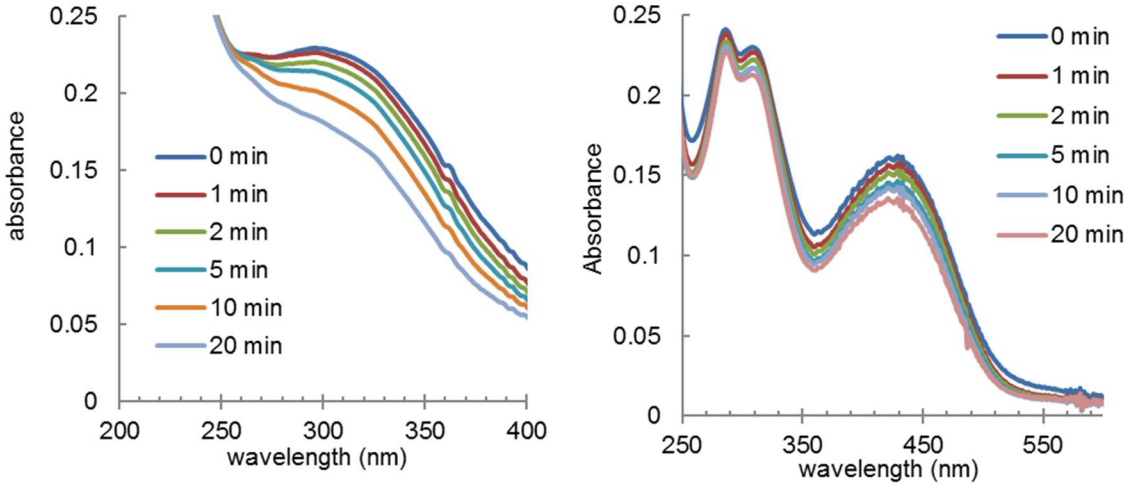

Figure 2.16 Top: Evolution of UV-vis spectra of C8-diCN-PPV doped with 15 wt.% DABCO with increasing (accumulated) illumination time. Bottom: Evolution of UV-vis spectra of RO-diCN-PPV doped with 15 wt.% DABCO with increasing (accumulated) time.

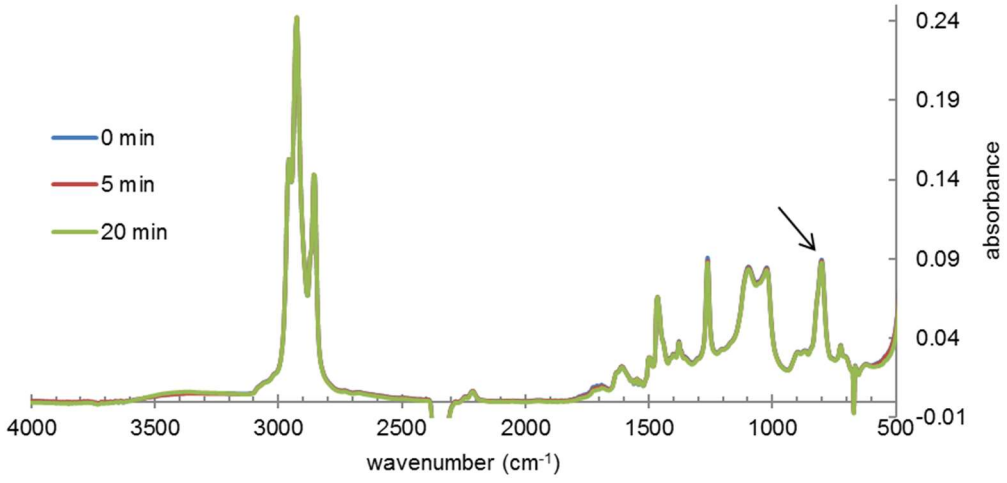

Figure 2.17 IR spectra of C8-diCN-PPV with 15 mol% DABCO illuminated for 0, 5, and 20 minutes. The integrated area for the alkyl peak between 2350 and 3100 cm-1 did not change after 20 minutes.

With DABCO doping, the RO-diCN-PPV degradation rate actually increased by 246% in the first 3 minutes of illumination and then slowed (Figure 2.16 bottom and Figure 2.18). The IR spectra (Figure 2.19) shows that the DABCO was consumed during the illumination. It is likely that RO-diCN-PPV, with a HOMO level (–6.04 eV), significantly lower than that of DABCO (–4.9 eV), can upon photoexcitation, oxidize DABCO into its radical cation.[44-45] DABCO radical cations are very reactive[45] and can initiate a radical process to degrade itself and the side chain in RO-diCN-PPV, as evidenced by a notable loss (3% in 5 minutes and 4% in 20 minutes) in the integration of C-H stretching peaks between 2350-3100 cm^{-1}, and the observation of a phenolic OH peak at 3400 cm^{-1} (Figure 2.19). The degradation of the vinylene units in the backbone does not result in the formation of any carbonyl groups due to the lack of protons on the vinylene units in the backbone. The mechanism is discussed in detail in chapter 3.

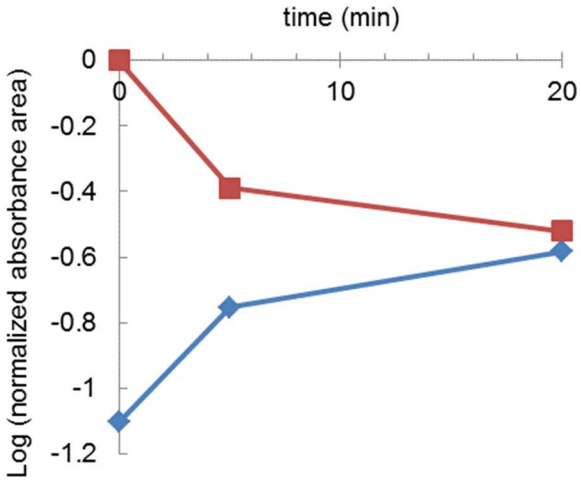

Figure 2.18 Peak integration of CH (between 2350-3100 cm-1) (red) and phenolic OH (between 3100-3600 cm-1) (blue) versus illumination time for RO-diCN-PPV with 15 mol% DABCO. The CH plot and OH plot mirror each other, indicating a correlation between the two groups

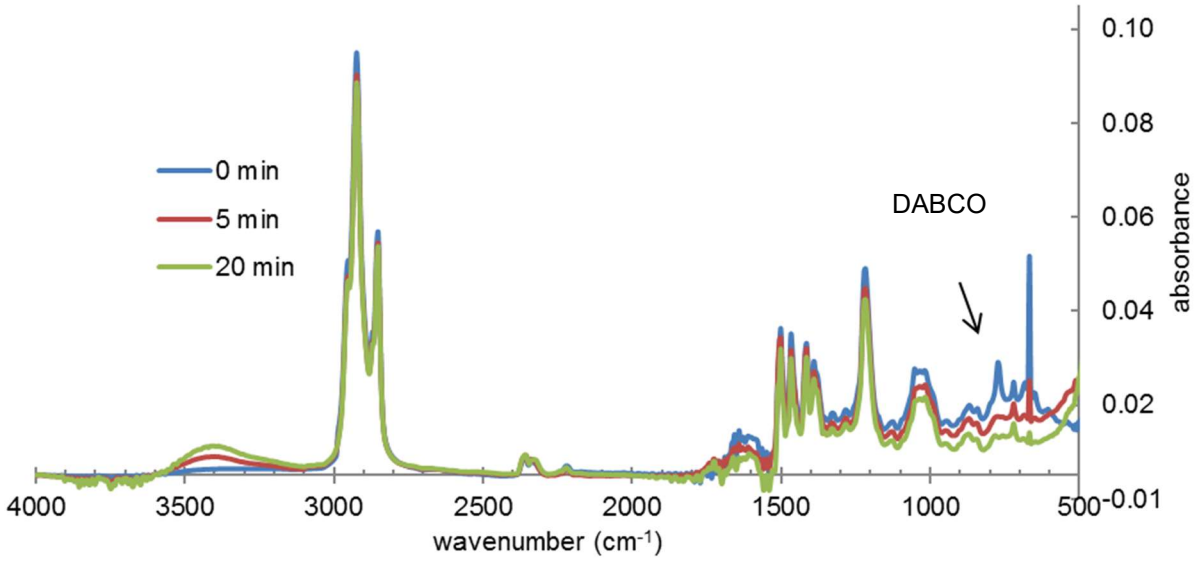

Figure 2.19 IR spectra of RO-diCN-PPV with 15 mol% DABCO illuminated for 0, 5, and 20 minutes. The Integrated area of the alkyl peak between 2350 and 3100 cm-1 decreased by 3% after 5 minutes and 4% after 20 minutes.

When the polymer absorbs light, an electron is promoted to the excited singlet state. In the excited singlet state the electron can undergo multiple processes including nonradiative decay, radiative decay (fluorescence), and intersystem crossing which forms the excited triplet state. The polymer in the excited triplet state can relax either through radiative decay (phosphorescence) or through an energy transfer to triplet oxygen.[43] The energy transfer to triplet oxygen leads to generation of singlet oxygen which initiates a sequence of decomposition reactions as shown in Scheme 2.3. First, a singlet oxygen reacts with the C=C via a 2+2 cycloaddition to form a dioxetane intermediate which undergoes rearrangement to form two oxo-acetonitrile groups.[41, 46] The resulting oxo-acetonitrile compound can easily hydrolyze with moisture in the air[40] to yield the main carboxylic acid degradation product observed in the IR analysis. This reaction sequence leads to cleavage of the vinylene bond of the polymer chain and a reduction in conjugation length.

Scheme 2.3 Photodegradation mechanism of C8-diCN-PPV and RO-diCN-PPV. Singlet oxygen attacks the double bond via 2+2 cycloaddition, followed by hydrolysis of the oxo-acetonitrile to the corresponding carboxylic acid.

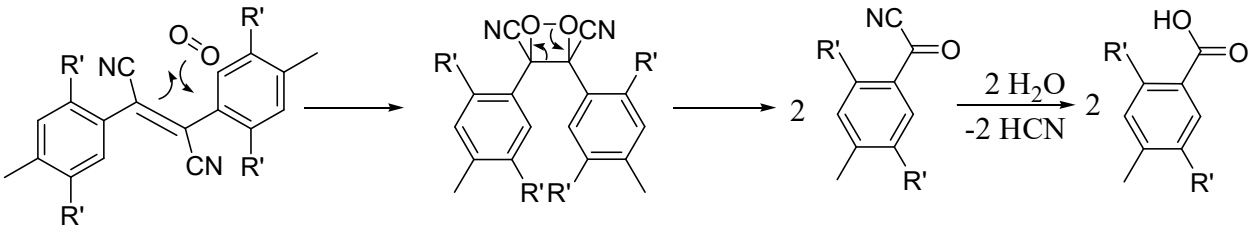

2.4 CONCLUSION

The synthesis of RO-diCN-PPV and C8-diCN-PPV has been modified to avoid formation of the imide structure. The LUMO level of the C8-diCN-PPV polymer is lower than RO-diCN-PPV by 0.15 eV. Despite the lower LUMO level, C8-diCN-PPV photodegrades seven times faster than RO-diCN-PPV. C8-diCN-PPV is found to be phosphorescent and the phosphorescence can be partially quenched by oxygen in air generating singlet oxygen. The singlet oxygen reacts with the vinylene backbone of the polymers and causes faster photodegradation. In C8-diCN-PPV, the LUMO level of the polymer is below that of oxygen, the radical degradation mechanism is less likely and the singlet oxygen pathway becomes dominant due to the presence of an efficient intersystem crossing process.

In RO-diCN-PPV, the LUMO level measured using CV (–3.54 eV) is barely higher than that of oxygen (O_2) (-3.59 eV) and the true LUMO level should be slightly lower than that of O_2 since CV measurement tends to give wider energy gaps due to overpotential. So in both polymers, the oxygen anion mechanism, which requires an electron transfer from the excited polymer to O_2 and is responsible for photo-oxidation of simple alkoxy-substituted PPVs, is not possible for both diCN-PPVs.

The IR analysis results of photodegraded films suggest that singlet oxygen is mainly responsible for the slow degradation of RO-diCN-PPV, and photoinduced superoxide radical anion generation does not happen or is not efficient. The sufficiently low LUMO level and absence of a fast intersystem crossing process are the reasons for the excellent photostability of RO-diCN-PPV. The correlation between intersystem crossing and side chain structure still remains unclear. Better understanding of the

dependence of intersystem crossing rate on molecular structure is needed to improve molecular design for better photostability of π-conjugated organic materials.

Chapter 3 Opposite Effects of a Singlet Oxygen Quencher on Photochemical Degradation of DiCyano-Substituted Poly(Phenylenevinylenes) With different Side Chains

3.1 INTRODUCTION

Π-Conjugated organic materials have many (potential) applications such as photovoltaics, light emitting diodes, solid-state dye lasing, biological imaging and sensing, and chemical sensing. However, photochemical stability is a major concern for these materials.[47-51] For electron-rich polymers, such as poly(3-hexylthiophenes) and poly(p-phenylene-vinylenes) (PPV), a radical degradation mechanism has been established.[30-32, 52] When illuminated in the presence of oxygen, the polymer donates an electron through charge transfer to an oxygen molecule to form a polymer cation and a superoxide radical anion. In the case of PPVs, the superoxide radical anion can abstract a hydrogen from a side chain to form a carbon radical.[31] It can also attack a vinylene unit in the backbone to produce a peroxide anion and a carbon radical.[31] Hoke et al. and Dam et al. have shown that the LUMO (lowest unoccupied molecular orbital) energy of a polymer is directly related to the rate of photodegradation.[24, 33] In our earlier reports, poly[2,5-bis(decyloxy)-1,4-phenylene-1,2-dicyanovinylene] (RO-diCN-PPV), and poly(2,5-dioctyl-1,4-phenylene-1,2-dicyanovinylene) (C8-diCN-PPV)[26, 53] were shown to have photostability up to 250 times that of RO-PPV, due to reduced LUMO energy, –3.54 eV and –3.69 eV as compared to –2.91 eV of RO-PPV. Superoxide radical generation was shut down in these two polymers,[53] however, singlet oxygen mechanism, though less aggressive, still limited their photostability, and C8-diCN-PPV degraded seven times faster due to faster $^1O_2$ generation in the polymer.

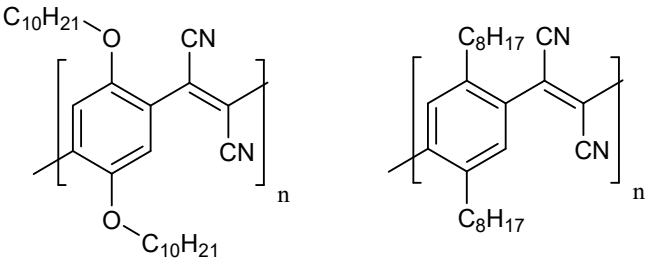

RO-diCN-PPV **C8-diCN-PPV**

Figure 3.1 Chemical structures of two diCN-PPV polymers**.**

For organic materials that undergo photodegradation via radical oxidation mechanisms, radical scavengers can be used to slow down the processes.[54-55] For materials that are sensitive to singlet oxygen, $^1O_2$ quenchers such as 1,4-diazabicyclo[2.2.2]octane (DABCO)[56] and other tertiary amines[43] are effective antioxidants and can be used to improve the lifetime of dyes in dye lasers and fluorescence microscopy,[57] as they can physically remove the excitation energy from $^1O_2$ without undergoing permanent change themselves and convert the energy to heat.[58]

In this work, the effects of DABCO on the photostability of RO-diCN-PPV and C8-diCN-PPV were investigated. To our surprise, the singlet oxygen quencher affected photodegradation of the two similar polymers in opposite ways, a situation not have been found in the literature. The differences in the mechanisms are elucidated with the help of UV-vis absorption and infrared spectroscopic methods, and molecular weight analysis.

3.2 EXPERIMENTAL

The polymer films were spin-coated from polymer solutions in *o*-dichlorobenzene on glass substrates for UV-vis measurements and drop casted on KBr plates for IR measurements. The optical density of the films on glass substrate was kept between 0.2 and 0.3, except when shown otherwise. Films on KBr plates are about 10 times thicker as

polymer absorption is about one order of magnitude weaker in the infrared (4000 - 650 cm^{-1}) than in the visible region.

A high power Newport light source (model 66903) equipped with a 300 W xenon arc lamp and a Newport power supply (Model 69911) was used for the photostability study. The xenon lamp produces light of broad spectrum from 200 nm to IR. The unfiltered output was focused on sample to generate an intensity of 2200 mW/cm^2, 22 times the intensity of one standard sun. UV-vis or IR analyses were performed immediately after illumination.

UV-vis spectra were obtained from an Agilent 8453 photodiode array UV-vis absorption spectrophotometer. Infrared spectra were obtained on a PerkinElmer Spectrum Two FT-IR spectrometer with a DynaScan interferometer, KBr optics and a temperature-stabilized DTGS detector. Molecular weights were determined using an Agilent 1100 series HPLC system, equipped with a diode array detector and two GPC columns (PL1110-6500, PLGel 5 mm MIXED-C 7.5×300 mm). Polystyrenes were used as the standards for conventional calibration and tetrahydrofuran as the solvent.

3.3 RESULTS AND DISCUSSION

3.3.1Photostability

Photooxidation of the polymer film samples was monitored using UV-vis absorbance Figure 3.2 Since the light intensity and oxygen concentration are constant, the photodegradation follows the first order rate law,[53]

$$log\frac{A}{A_0} = -Kt, \qquad (3)$$

where K is the effective polymer photodegradation constant, A_0 is the initial peak absorbance, and A/A_0 is the normalized peak absorbance. Log (A/A_0) is plotted as a

function of time in Figure 3.4. The absolute values of the slopes are the effective degradation constants. Since decomposition product can have absorption tailing into the peak region of the polymer and causes the data points to deviate from a linear dependence as the illumination continues. This effect is much more significant in the pristine C8-diCN-PPV film than other samples. Therefore, in Fig. 4, only the data points in the first 5 minutes are used to calculate the slope for C8-diCN-PPV. The initial photooxidation rate of C8-diCN-PPV is 7 times greater than that of RO-diCN-PPV.

With 15 mol% DABCO doping, the degradation rate of C8-diCN-PPV film decreased by 65% Figure 3.2 in consistency with the singlet oxygen mechanism. The effect of DABCO in RO-diCN-PPV may not appear significant when comparing the top two charts of Figure 3.3. After the spectra are magnified (Figure 3.3 bottom), it becomes clear that, with DABCO doping, the degradation of RO-diCN-PPV was much faster in the first 3 minutes of illumination and then slowed. Comparing the slopes of doped RO-diCN-PPV in the first 3 minutes and the undoped Figure 3.4, the initial decay rate of doped sample was faster by 246%.

3.3.2 Characterization of Photodegradation Products

To understand the different effects of DABCO, IR spectroscopy was used to examine components and functional groups evolution during the course of illumination.

C8-diCN-PPV. IR spectra of the undoped and doped films with different illumination time are in shown in, and the following observations are made:

1) The integrated area of the C–H peaks of the doped sample during 20 min of illumination remained constant, just as the undoped sample, consistent with a singlet oxygen mechanism.

2) The formation of COOH (with C=O at 1716 and OH at 3425 cm^{-1}) and oxo-acetonitrile [C(O)CN with C≡N at 2244 and C=O at 1768 cm^{-1}, a product of $^1O_2$ cleavage of the dicyanovinylene and the precursor of COOH[13]] and the loss of the vinylenyl CN (2223 cm^{-1}) are all slower in the

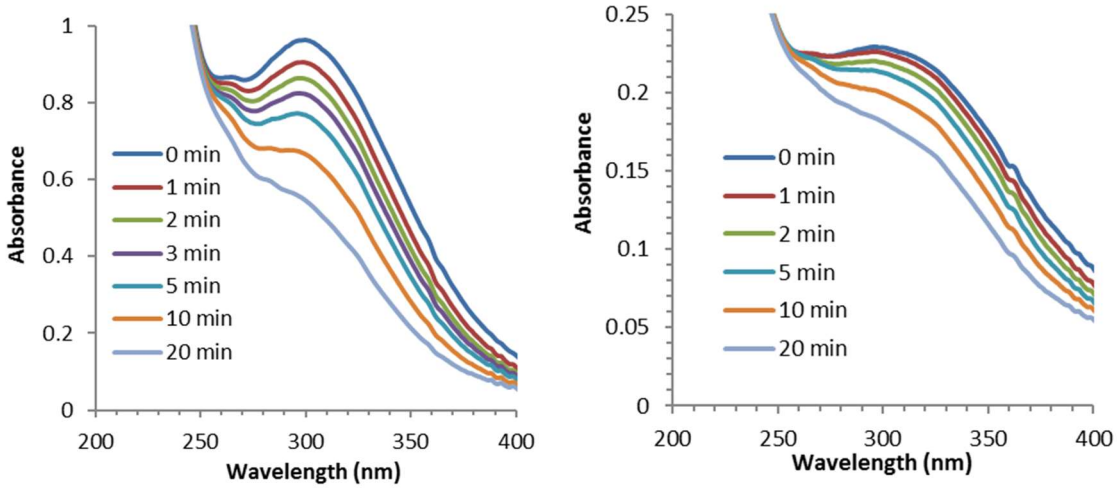

Figure 3.2 Evolution of UV-vis spectra of C8-diCN-PPV film (left) and C8-diCN-PPV film doped with 15 mol% DABCO with illumination time. DABCO has some absorption at 260 nm, which causes the polymer peak at 300nm in the doped film to appear weaker.

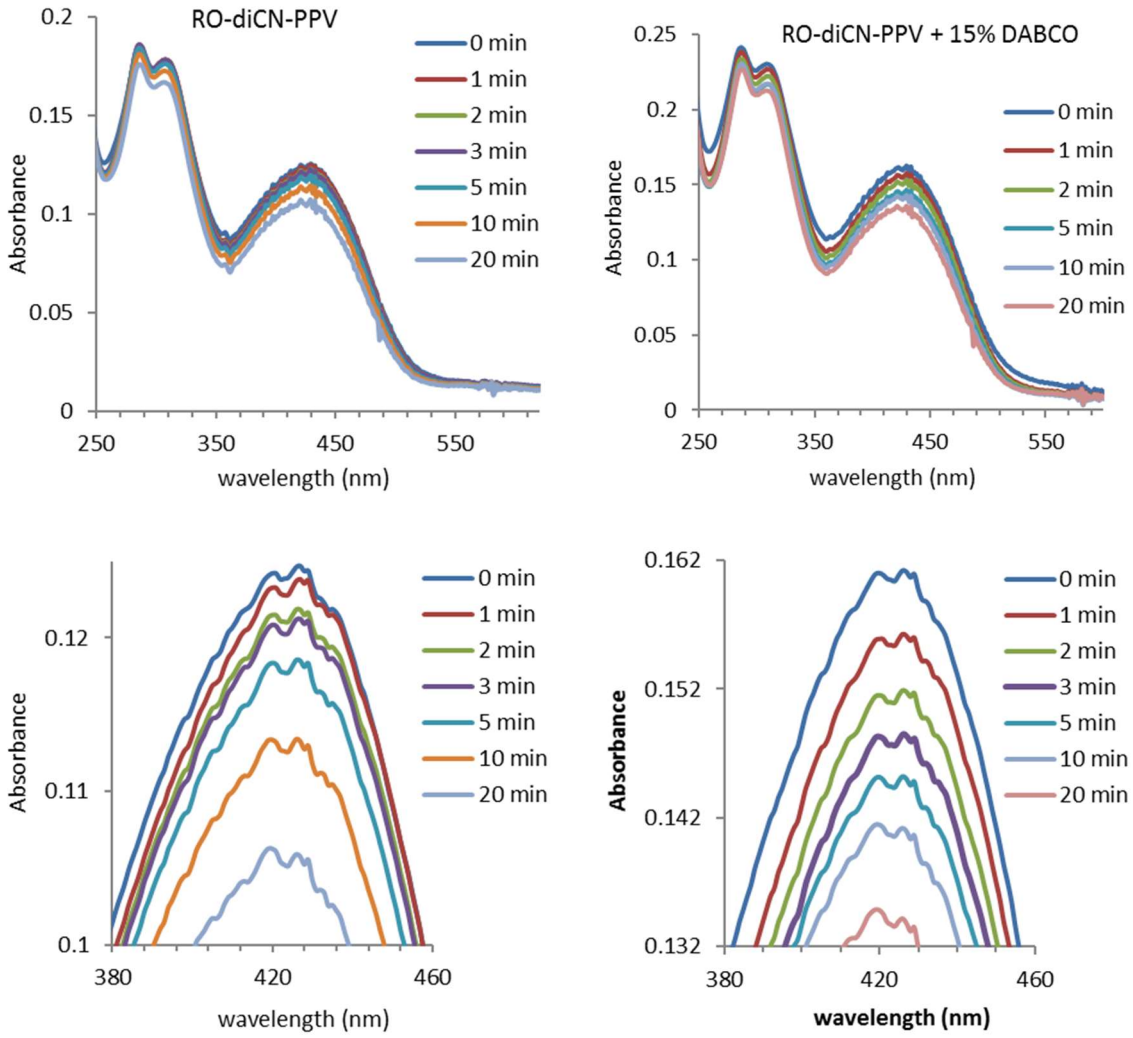

Figure 3.3 UV-vis spectra of RO-diCN-PPV film (top left) and 15 mol% DABCO-doped RO-diCN-PPV film (top right) with increasing illumination time. Bottom are expanded views of the top plots to show that degradation is significantly faster in the doped film in the first few minutes.

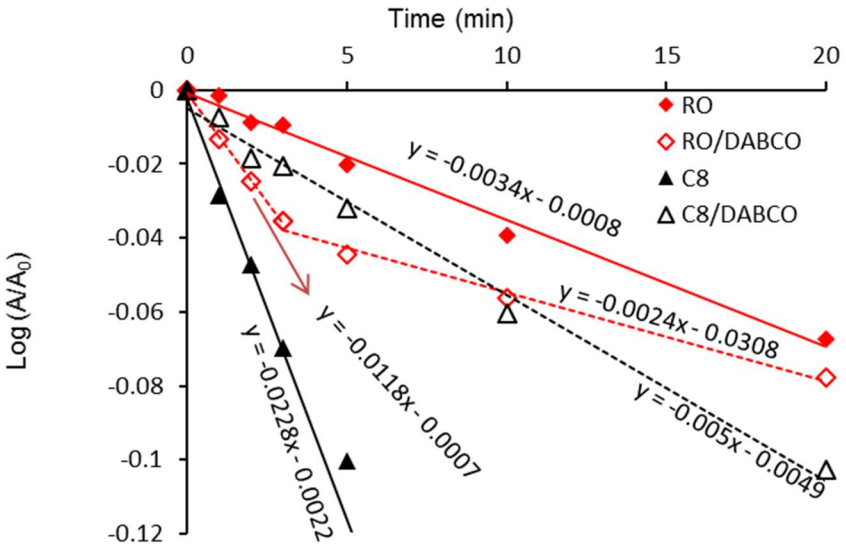

Figure 3.4 Semilog plots of normalized peak absorbance vs. illumination time**.**

doped sample in agreement with the slower degradation observed in the UV-vis measurements. This further supports the singlet oxygen mechanism because DABCO is a singlet oxygen quencher and there is no report on its ability to inhibit a radical process.

3) The DABCO in the doped sample was not consumed during the 20 minutes of illumination, in stark contrast to the fate of DABCO in RO-diCN-PPV. This observation also helps exclude the involvement of a radical process as it is known that DABCO reacts with oxygen and other free radicals.[59]

4) The C(O)CN carbonyl peak (1768 cm^{-1}) is as strong as the COOH carbonyl peak (1716 cm^{-1}) in both samples, while the same signal in the earlier report[53] of the undoped sample only appeared as a shoulder of the COOH carbonyl peak. This is because C(O)CN is not stable in film and IR measurements in this study were performed with less delay after illumination (< 1 minute opposed to 5-10 minutes). Previously, it was noted that C(O)CN hydrolyzed completely when the illuminated films were transferred from slides to KBr plates using a solvent (CH_2Cl_2).[53]

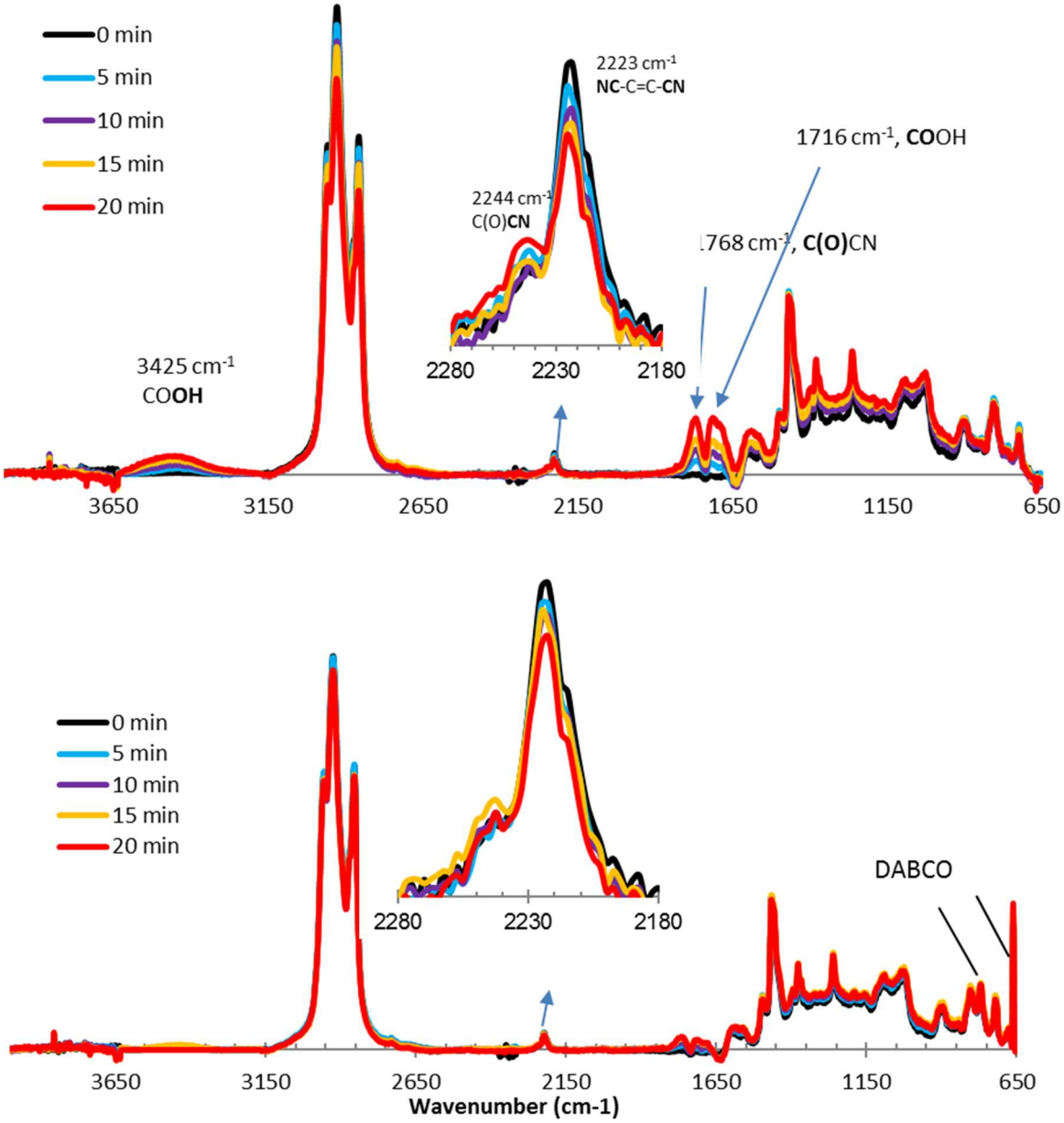

Figure 3.5 IR spectra of C8-diCN-PPV without (Top) and with (Bottom) 15 mol% DABCO illuminated for 0, 5, 10, 15 and 20 minutes.

RO-diCN-PPV. The IR spectra of the pristine and 15 mol% DABCO-doped polymer samples with different illumination time are shown in Figure 3.6. Hardly any change happened to the undoped RO-diCN-PPV, showing again the excellent photostability of this polymer.[53]

The following changes happened to the doped sample after illumination:

1) 80% loss of DABCO after 5 minutes of the illumination and complete loss at 20 minutes.

2) A notable loss (3%) in C–H in 2350-3100 cm^{-1} and a gain in O–H in 3100-3600 cm^{-1} after the first 5 minutes. In the next 15 minutes, only 1% degradation of C–H was observed. The OH peak was not from COOH since no peak rose in the carbonyl region (in other words, COOH was not produced).

3) Partial loss of the original CN peak intensity and rise of a new CN peak at 2243 cm^{-1} mostly in the initial 5 minutes (Inset of Figure 3.6 bottom). The new CN peak, which is not from oxo-acetonitrile as no peak rises in the carbonyl region, is assigned to product **Q** in Scheme 3.2, which has two cyano-containing moieties: cyanohydrin and phenylacetonitrile. The peak position is close to those of naththalenyl cyanohydrin (2248 cm^{-1})[60] and phenylacetonitrile (2252 cm^{-1}). From the relative peak intensities of vinylenyl cyano (2216 cm^{-1}) and the cyano groups of **M** (2243 cm^{-1}) (in the inset of Figure 3.6), the amount of decomposed vinylene units is estimated to be 26% (or on average 4 units per polymer chain) at 5 minutes. The change after 5 min was much slower.

Are phenolic products generated in DABCO-doped RO-diCN-PPV? In photodegradation of RO-PPV, both carboxylic acid and phenolic products are produced and give a broad

peak around 3400 cm^{-1}.[52] For DABCO-doped RO-diCN-PPV, carboxylic acid products have been ruled out. To help determine the presence of phenolic products in DABCO-doped RO-diCN-PPV, a 15 mol% p-methoxyphenol doped RO-diCN-PPV sample was studied by IR spectroscopy. Three peaks involving phenolic OH are identified at 3420, 1511, and 1227.5 cm^{-1} and are labeled on the spectrum (Figure 3.6). The 1227.5 cm^{-1} peak is

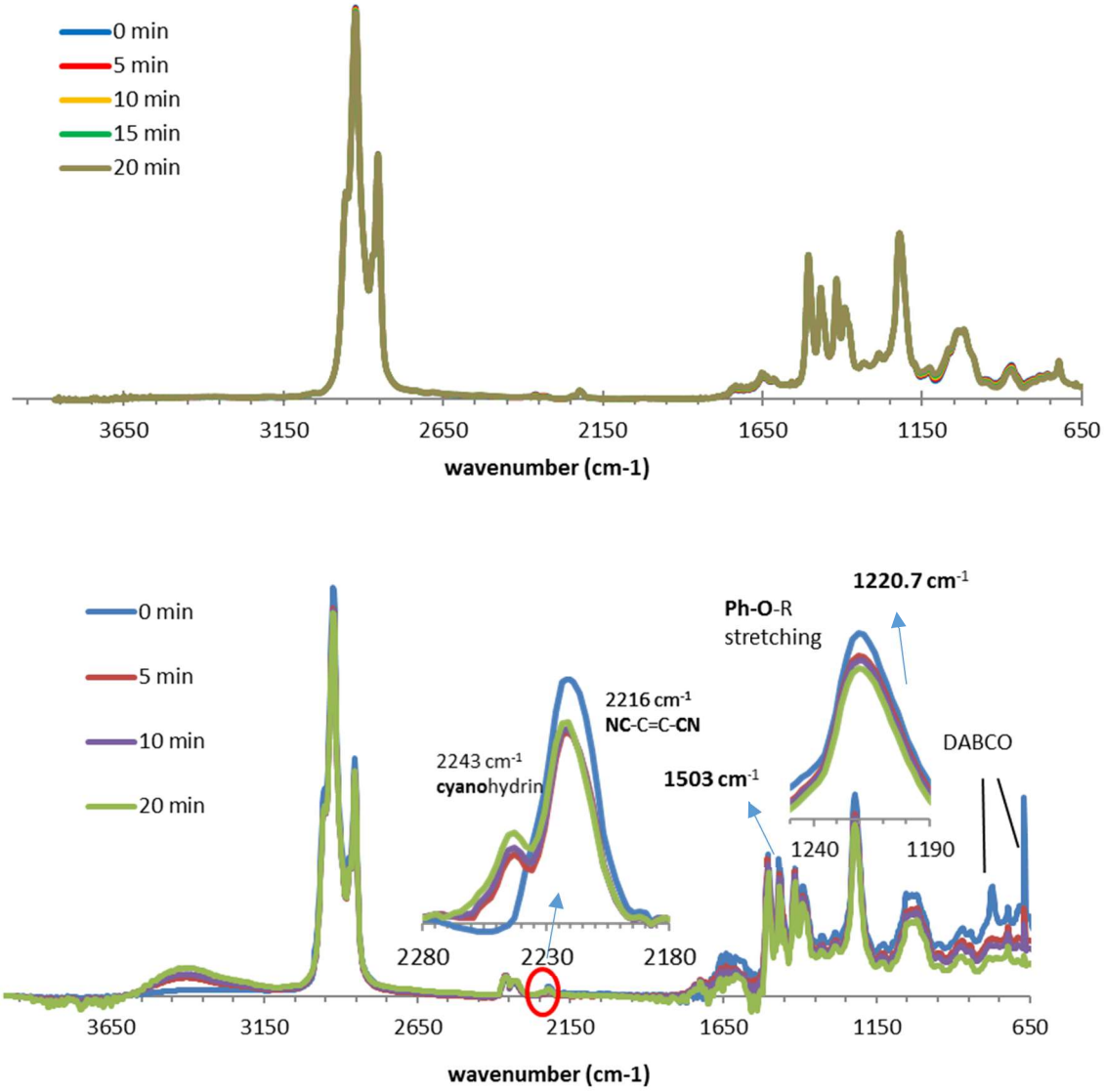

Figure 3.6 IR spectra of RO-diCN-PPV without (Top) and with (Bottom) 15 mol% DABCO illuminated for different time. The apparent stronger signal of 0 min sample around 1650 cm-1 is due to the more tilted baseline.

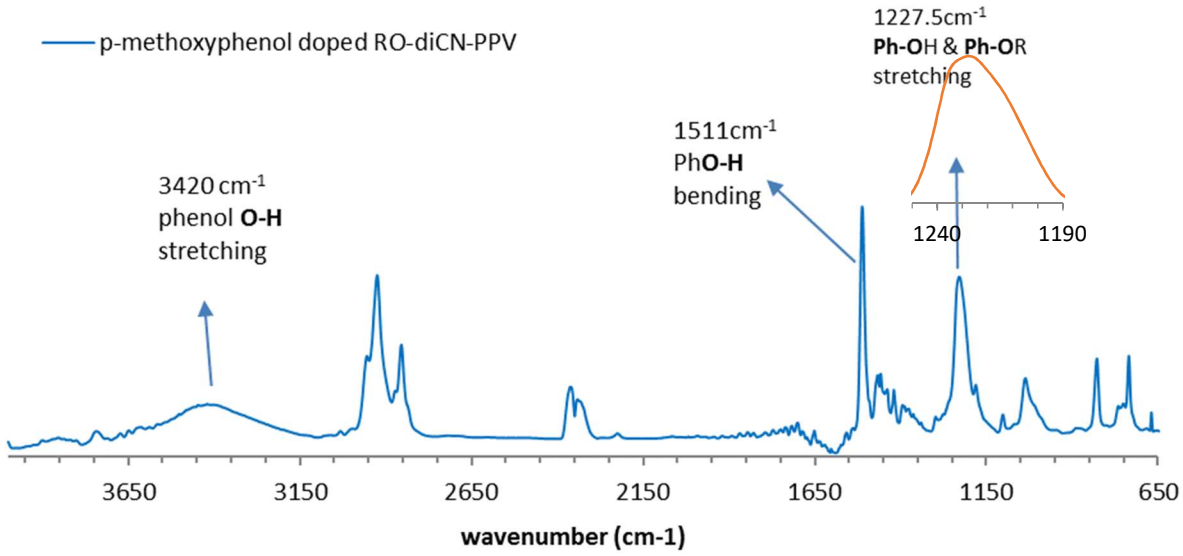

Figure 3.7 IR spectrum of 15 mol% p-methoxyphenol doped RO-diCN-PPV, showing that phenolic OH is involved in three peaks at 3420, 1511, and 1231 cm^{-1}. The 1231 cm^{-1} peak overlaps with the stretching peak of Ph-OR of RO-diCN-PPV (1220.7 cm-1) to give a broad peak at 1227.5 cm^{-1}.

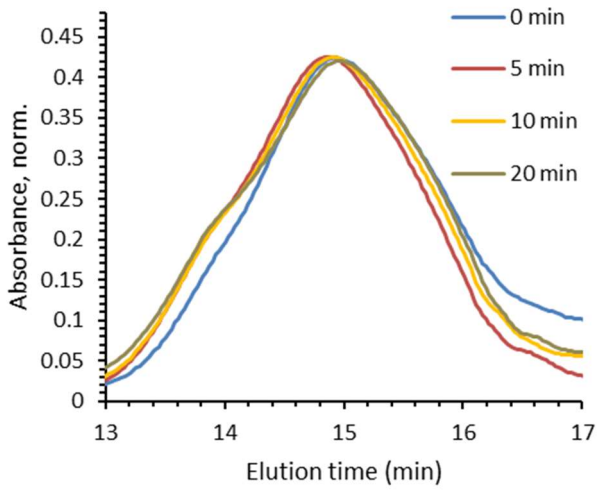

Figure 3.8 GPC elugram of 15 mol% DABCO-doped RO-diCN-PPV illuminated for different time. Wavelength of detector: 310 nm. The right-hand high tail of 0 min elugram was not from the polymer as the tail did not show up in the GPC curve monitored at 440 nm.

an overlap of C–O stretching of Ph–OH (1231 cm^{-1}) of the dopant[59] and Ph-OR of RO-diCN-PPV (1220.7 cm^{-1}, inset in Figure 3.6 bottom). In the IR spectra of DABCO-doped RO-diCN-PPV (Figure 3.6 bottom), no indications of phenolic OH, i.e., intensity increase at/near 1511 cm^{-1} and broadening/shift of the 1220.7 cm^{-1} peak, are found. So, phenolic products were not produced in photodegradation of DABCO-doped RO-diCN-PPV.

GPC study of DABCO-doped RO-diCN-PPV. Changes in GPC elugrams with illumination time are notable when the plots are zoomed into the peak area (Figure 3.8). First, after 5 min illumination a shoulder peak appeared on the left slope at the elution time of 13.78 minutes, corresponding to a peak MW (M_p) of 29,000 which is 3.7 times the M_p of the pristine RO-diCN-PPV, and the shoulder peak stayed after further exposure to light. Second, the peak retention time decreased from 14.93 minutes (M_p = 7,800) for

the fresh sample (0 min) to 14.88 minutes (M_p= 8,400) for the 5 min sample. Further illumination caused the retention time to increase to 14.90 minutes (M_p = 8,100) for the 10 minutes sample and 14.97 minutes (M_p = 7,500) for the 20 minutes sample. These observations clearly indicate that a radical process, which increases MW by radical combination and radical addition, happened in the first five minutes, and yielded the dominance to a singlet oxygen mechanism, which reduced MW by cleaving C=C bond,[53] when DABCO was mostly consumed.

3.3.3 Radical photodegradation mechanism of DABCO-doped RO-diCN-PPV

The above observations of DABCO-doped RO-diCN-PPV indicate that a radical process was introduced by DABCO and dominated the photodegradation before DABCO was mostly consumed. To illustrate what happened between diCN-PPVs and DABCO upon illumination, molecular frontier orbitals energy[13] diagram, and photoexcitation and electron transfer processes are shown in Figure 3.9. With a HOMO level (–6.04 eV), lower than that of DABCO (–4.9 eV[61], or –5.07 eV from our CV measurement), RO-diCN-PPV can oxidize DABCO into a radical cation upon photoexcitation.[45, 61] Photoinduced electron transfer (PET) to other molecules such as carbonyl compounds to form reactive radical cations,[44, 62-63] has been documented for tertiary amines. Amine radical cations are very reactive[61] and can degrade itself, the side chains and the vinylene units of RO-diCN-PPV via hydrogen abstraction, radical addition, and α-cleavage.[62-63] Relative to other tertiary amine radical cations, DABCO radical cation is significantly more stable and less acidic.[64-65] Nevertheless, it was shown that it can undergo acid-base reaction with a neutral DABCO and get converted into a carbon radical in the time scale of seconds in solutions (Scheme 3.2).[45]

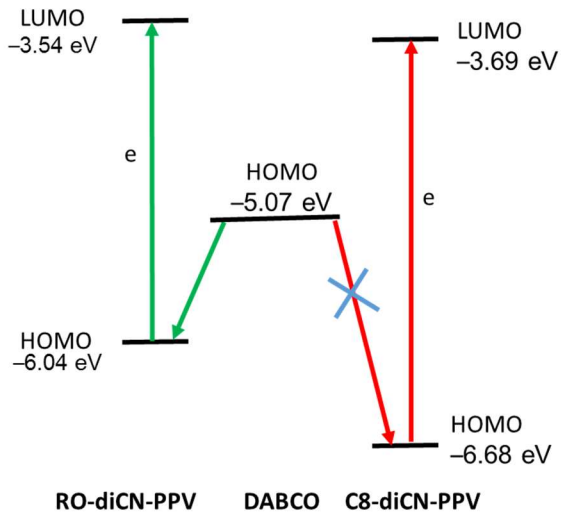

Figure 3.9 Energy diagram of diCN-PPVs and DABCO. Upon photoexcitation, an electron is promoted into the LUMO, leaving a hole in HOMO. An electron in the HOMO of DABCO can transfer efficiently to the hole of RO-diCN-PPV, but not to the hole of C8-diCN-PPV.

Apparently, the energy difference between the HOMO of C8-DiCN-PPV (–6.68 eV)[53] and the HOMO of DABCO is too large for an efficient electron transfer from DABCO HOMO to the polymer HOMO to occur. Therefore, DABCO doping does not introduce a radical process to C8-DiCN-PPV.

3.3.4 Radical reactions of the side chain in DABCO-doped RO-diCN-PPV.

Scheme 3.1 shows radical reactions of the alkoxy side chain, which is partially adapted from the literature.[52] The position α to the oxygen atom is well-known for its high reactivity.[52, 66] A hydrogen on an α carbon may be abstracted by a DABCO cationic radical or an oxygen radical generated during the radical process (Scheme 3.2) to form a carbon radical **B**. Two possible reactions may happen to **B**: addition to a vinylene unit (the blue path in Scheme 3.1) and/or reaction with O_2 to form a peroxy radical **C** (the red

path adapted from that for RO-PPV).[52] The red path would led to production of ester **F** (~1760 cm^{-1}), formate **G** (1740 cm^{-1}), phenol **I**, and aliphatic acids (~1732 cm^{-1}). However, no evidences of their presence are found in the IR spectra of DABCO-doped RO-diCN-PPV (Figure 3.6, bottom). So, the red path is not active for RO-diCN-PPV. This is unexpected but justifiable because the dicyanovinylene is a much stronger radical receptor than the vinylene in RO-PPV as electron withdrawing groups can greatly increase the reactivity of alkenes for radical addition.[67] For example, a cyano substitution increases radical addition reaction rate of ethylene by 174 times. Radical **B** may add to vinylene intra- or intermolecularly. The intermolecular addition was at least partially responsible for the increase in polymer MW.

3.3.5 Radical reactions of the backbone.

In DABCO-doped RO-diCN-PPV, loss of absorbance is due to attack of radicals at the vinylene units. The mechanism outlined in Scheme 3.2 is adapted from that proposed by Chambon et al. for RO-PPVs.[30-31] The DABCO cationic radical (**a**) is acidic and can be deprotonated by a DABCO to form a carbon radical **c**.[45] The radical process could be initiated by different radicals including **a**, **B**, **c**, and possibly other radicals that were generated during the radical process. The rest of the pathway is different from that of RO-PPV[30-31] in two ways: 1) the radical intermediate **N** could not do a cage reaction,[31] which is favored reaction if a hydrogen is present instead of a CN, and 2) N did not undergo β-scission (cleavage of the red colored bond in **N**, a significant way of evolution of alkoxy radicals[5228]) since no carbonyl peak (from **P**) was observed. Radical **N** abstracts a hydrogen from a hydrogen source to form the cyanohydrin **Q** which is quite stable.[26]

The OH in cyanohydrin is responsible for the broad OH peak (3100-3600 cm^{-1}) (Note: OH in naphthalenyl cyanohydrin peak at peak near 3418 cm^{-1}).[60]

Scheme 3.1. Radical reactions of the alkoxy side chains of RO-diCN-PPV doped with DABCO. R′• = DABCO radical cation or an oxygen radical.

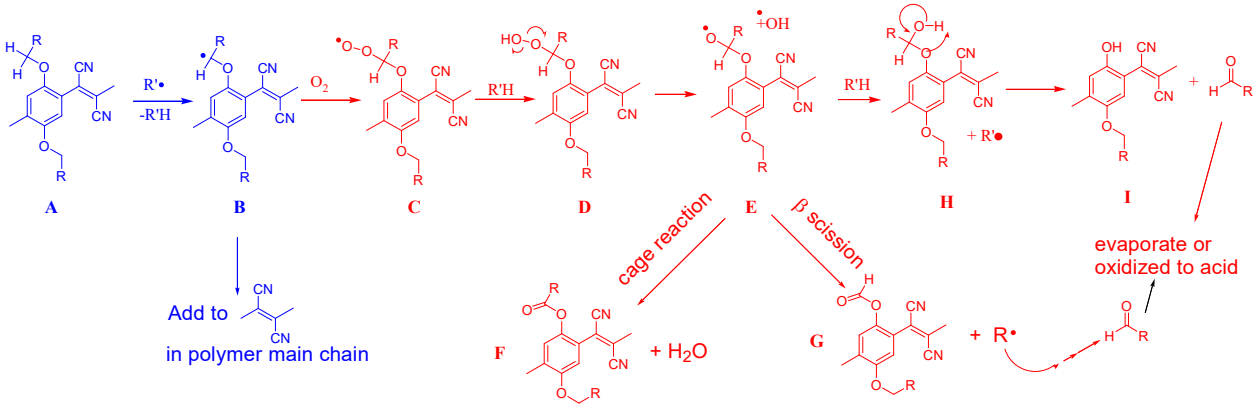

Scheme 3.2 Radical degradation of vinylene backbone in RO-DiCN-PPV initiated by the radical cation of DABCO. R′• = DABCO radical cation (**a**), **B**, **c**, or other radicals that were generated during the radical process.

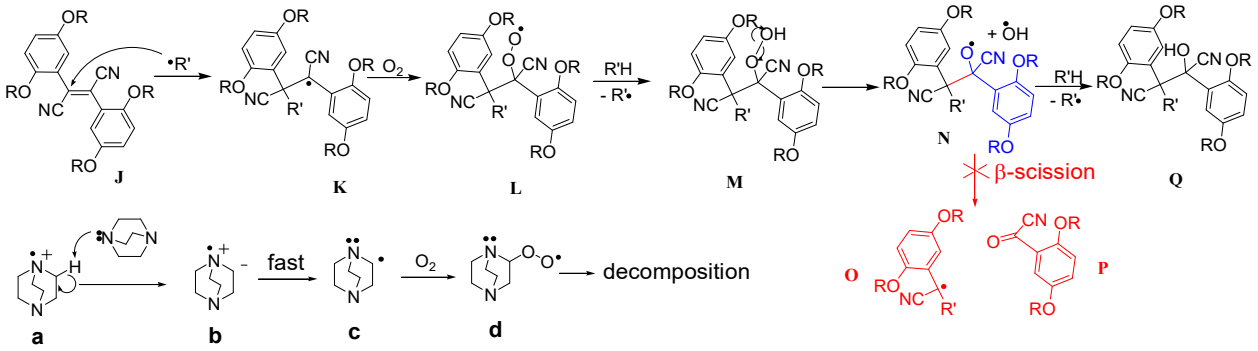

The PET between RO-diCN-PPV and DABCO also produced polymer radical anions which is similar to **K** and may follow the same path in Scheme 3.2 to eventually give a product similar to **Q**. The anion can obtain a proton from a DABCO cationic radical (**a**) to turn into a neutral radical

3.4 CONCLUSIONS

The effects of DABCO on the photostability of RO-diCN-PPV and C8-diCN-PPV were investigated. To our surprise, the singlet oxygen quencher had opposite effects on photodegradation of these two polymers. With 15 mol% DABCO doping, degradation rate of C8-diCN-PPV film decreased by 65%, while the degradation rate of RO-diCN-PPV increased by 246% in the first 3 minutes of exposure to intense white light and then slowed, as indicated by UV-vis absorption. IR experiments showed that DABCO content in C8-diCN-PPV film remained unchanged during 20 minutes of illumination, but lost 80% in RO-diCN-PPV in only 5 minutes. With the loss of the most of DABCO, degradation of vinylene units and loss of CH immediately slowed down.

All the IR and GPC MW analysis results suggest that DABCO slowed down degradation of C8-diCN-PPV without altering the degradation mechanism, but accelerated RO-diCN-PPV photodegradation and switched the dominant mechanism from singlet oxygen to radical oxygen. The difference arises from the difference in their side chains. The alkoxy in RO-diCN-PPV donates electron and raise the HOMO energy from -6.68 eV for C8-diCN-PPV to -6.04 eV, which is still lower than the HOMO of DABCO, but not too low to shut down electron transfer from the HOMO of DABCO to the HOMO of RO-diCN-PPV where holes are generated upon photoexcitation. The result of IR product analysis indicates that the side chain carbon radicals did not follow the usual path (i.e., reacting with O_2 and eventually getting cleaved), but rather added to the dicyano substituted C=C bonds. One consequence of the deviation(s) from the side chain radical decomposition of RO-PPV is that the broad OH IR peak is now assigned to cyanohydrin – a decomposition product of dicyanovinylene, rather than phenols and carboxylic acids that are generally produced in radical decomposition of RO-PPVs.

Mechanisms have been modified to rationalize the observed differences from radical decomposition of RO-PPV.

The study presents an interesting case where addition of a singlet oxygen quencher produces opposite effects on photodegradaton of two polymers that are only different in side chain.

ACKNOWLEDGEMENTS

This material is based upon work supported by the U.S. Air Force Office of Scientific Research under Award No. FA955010-1-0555 and South Dakota NSF EPSCoR Program (Grant No. 0903804). LS is grateful for the funding from NSF SD IGERT at U. South Dakota (Grant No. 0903685)

Chapter 4 A Mechanistic Study of the Photodegradation of Poly(3-hexylthiophene-2,5-diyl) and Poly(3,5-didodecyl-cyclopenta[2,1-b;3,4-b']dithiophen-4-one)

4.1 Introduction

There has been intense research over the past decade into polymers for use in photovoltaic devices. Polymer Solar cells (PSCs) have many advantages over traditional solar cells, such as; mechanical flexibility, portability, and low manufacturing costs.[1-2] Power conversion efficiencies have surpassed 10%.[68] One of the main hurdles for the use of organic polymers in photovoltaics and other applications is the photostability of the active material, whichlimits the useful lifetime of the device.[29, 47-49, 69] To date, the most photostable PSC module has a t_{80} (time it takes to reach 80% of initial efficiency) of ~10,000 h or 3.4 years, this is far below the target lifetime of 15 years.[27] When the polymers in PSCs photodegrade, they lose their mechanical and, more importantly, their optical properties. To better understand how conjugated polymers degrade in sunlight, two polymers with slight structural differences were compared. Poly(3,5-didodecyl-cyclopenta[2,1-b;3,4-b']dithiophen-4-one) [C_6-CPDTO] is a polymer that has recently been synthesized in our group, it is similar in structure to P3HT but contains a ketone that fuses two adjacent thiophene units. Cyclopenta[2,1-b;3,4-b']dithiophen-4-one (CPDTO) is a structural unit that shows promise for use in photovoltaic applications, it has a low bandgap (1.1-1.2 eV) as a homopolymer.[70] polyCPDTO that lacks side chains can only be synthesized in small quantities via electropolymerization and is not soluble, thus making processing impossible.[70] Substituted CPDTO polymers on the other had are very soluble but due to steric hindrance from the side chains, the structure is non-planar and the polymer loses its optical and electronic characteristics. C_6-CPDTO has alternating monomers with and without side-chains, reducing steric hindrance and allowing for a

more planar structure. The LUMO level of C_6-CPDTO is lower than that of P3HT, we compared its photostability to that of P3HT. As expected C_6-CPDTO degrades 2.5 times more slowly than P3HT.

There has been a lot of work focused on the photostability of polymers[29] and in particular P3HT[32, 69, 71-75] but many of these studies fail to look at the role that structure plays in the photostability of the substrate. This work is focused on studying the specific degradation mechanisms in a diverse group of functional polymers to better understand the interplay of structure and stability. Through better understanding of the structural-stability relationship of these polymers, we will be able to apply this knowledge to design polymers that are more photostable.

There has been debate on the mechanism that is responsible for the degradation of P3HT. Early reports have suggested that generation of singlet oxygen through photosensitization leads to the destruction of the polymer.[76-77] Later reports have shown that P3HT degrades through a radical degradation mechanism.[32, 72-75, 78] Abdou and Holdcroft suggest that it is a combination of radical degradation and singlet oxygen degradation,[79] and this is what was observed in this study. Radical degradation is initiated by the donation of an electron from the excited singlet state of P3HT to molecular oxygen. This process generates a radical cation polymer and a superoxide radical anion. In P3HT, the superoxide radical anion can abstract a hydrogen from a side chain, forming a carbon radical. This mechanism was confirmed in this study, but it was shown that it only degrades the side chain and oxidizes the sulfur of the thiophene unit. Radical degradation is not responsible for the loss of conjugation in P3HT, which is more likely due to degradation by singlet oxygen. Conversely, C_6-CPDTO does not degrade by

singlet oxygen and is only degraded by a radical degradation mechanism. The difference in mechanisms is likely due to the efficiency of intersystem crossing in P3HT compared to C_6-CPDTO.

4.2 Experimental

NMR experiments were conducted on Bruker Avance 400MHz and 600 MHz NMR spectrometers. The molecular weight of polymers was measured on an Agilent 1100 series HPLC system with ChemStation B.04.03 and GPC Data Analysis B.01.02, equipped with two serial GPC columns (PL1110-6500: PLGel 5 mm MIXED-C 7.5 × 300 mm). Polystyrenes were used as the standards for conventional calibration and tetrahydrofuran was used as the solvent. The polymer films were spin-coated from the polymer solutions in *o*-dichlorobenzene on glass substrates. UV–vis absorption spectra were obtained on an Agilent 8453 photodiode array UV–vis absorption spectrometer.

Photoluminescence (PL) was measured on a Perkin Elmer LS-50B luminescence spectrometer. All measurements were performed in air with no inert gas purging to protect film or solutions except where indicated. Measurements performed under nitrogen where carried out on a small glass slide affixed inside a quartz cuvette, which was sealed inside a nitrogen filled glovebox. The emission correction was performed in the range of 200-900 nm using deuterium-tungsten light source with known spectral distribution. A high power Newport light source (model 66903) equipped with a 300 W xenon arc lamp and a Newport power supply (Model 69911) was used for the photostability study. The output from the light source was used without filtering. Light Intensity was adjusted through a focus lens and measured by a Newport 70260 power meter with a 3A-P-SH –

V1 thermal head. The aperture diameter of the power meter is 1.2 cm and the unit intensity is calculated to be 2400 mM/cm^2, 24 times that of one standard sun intensity.

Infrared spectra were measured on a Perkin Elmer Spectrum Two FT-IR spectrometer with KBr Windows. The samples were drop coated on a KBr plate in ambient air. The samples were photodegraded on the KBr plate and IR analysis was done immediately after illumination. The spectra were collected at a resolution of 4 cm^{-1} and presented as an average of 5 scans.

Cyclovoltammetric measurements were performed on an eDAQ Potentiostat System (ER466 plus software EChem 2.1.5) equipped with platinum auxiliary and working electrodes and a silver reference electrode in a CH_3CN solution of $AgNO_3$ (0.01 M) and tetrabutylammonium hexafluorophosphonate, TBA-HFP (0.1 M). The polymer samples were dissolved in chloroform and then dip coated onto the Pt working electrode. The electrodes are housed in an 8-mL vial half-filled with TBA-HFP/acetonitrile solution (0.1 M). The solution was N_2-purged and a scan rate of 100mV/s was used. Between measurements, the surface of the electrodes were cleaned or polished. Ferrocene (2 mM in the electrolyte solution) was used as an internal reference standard and its HOMO level of –4.80 eV was used in calculations.

4.3 Results and Discussion

4.3.1 Optical properties

The absorbance and luminescence spectra of CPDTO and P3HT were measured and shown in Figure 4.1. P3HT has a characteristic absorbance peak at 510 nm, CPDTO absorption extends to 900 nm due to its lower band gap.

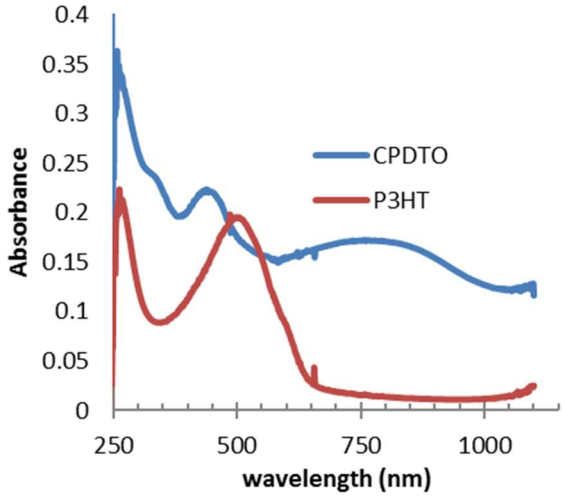

Figure 4.1 UV-Vis absorbance spectrum for C_6-CPDTO (Blue) and P3HT (Red) thin films.

4.3.2 Photostability

The UV-Vis spectra of CPDTO and P3HT were monitored after illumination with a xenon arc lamp. The xenon arc lamp has the intensity of 24 times that of 1 standard sun. This light source is used to accelerate the photodegradation of the polymers. The UV-Vis absorbance is indicative of the number of unsaturated bonds in the polymer. The change in the absorbance is also less affected by quenching and changes in morphology, as photoluminescence is. As the polymer degrades and conjugation is broken, the absorbance decreases. Figure 4.2 shows the decrease in absorbance of P3HT **A** and C_6-CPDTO **B**. The absorbance peak in P3HT decreases and blue shifts as the conjugation of the polymer is broken. The blue shift is indicative of shortening of the conjugation length. Oxidation of the sulfur in the thiophene ring would lead to the loss of aromaticity and introduce a donor-acceptor interaction leading to a red shift in light absorbance. However, no red shift was noted for either P3HT or C_6-CPDTO.

To compare the photostability of the two polymers, the rate of degradation needs to be determined. The decay rate can be expressed as $\frac{dC}{dt} = -kC \cdot I \cdot [O_2]$, where C is polymer concentration, I is light intensity, and $[O_2]$ is the oxygen concentration. Since $[O_2]$ and I are constant, the relation becomes pseudo first order. Subsituting absorbance A into the equation, it becomes $\frac{dA}{dt} = -kA$. From this equation we get $\frac{dA}{A} = -kt$ from which we derive $A = A_0 e^{-kt}$ which is the pseudo-first order rate expresson. K is the effective rate constant for the degradation of the polymer. A/A_0 is the normalized absorbance of the polymer. $Ln(A/A_0)$ is plotted as a function of total illumination time in Figure 4.3. This linearize the plot so a linear best fit line can be added to obtain the rate constant. The degradation rate is correlated with the destruction of conjugation in the polymers. From this plot we can see that P3HT degrades 2.5 times faster than CPDTO and they both follow pseudo-first order kinetics.

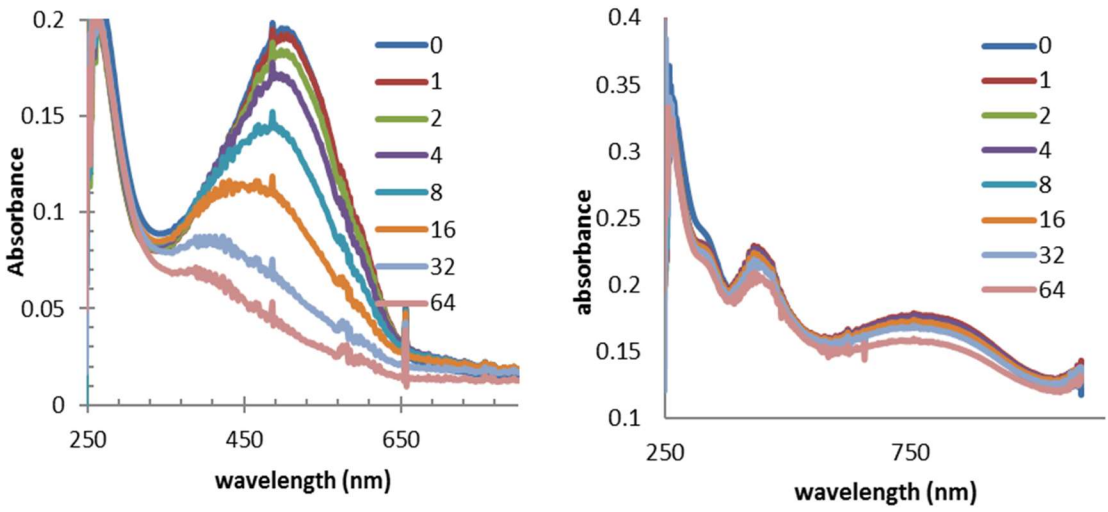

Figure 4.2 UV/Vis absorbance spectra for C_6-CPDTO (Left) and P3HT (Right) at accumulated illumination time in minutes

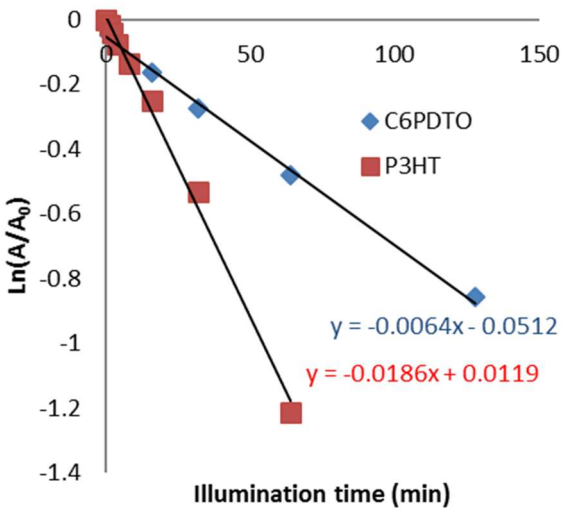

Figure 4.3 Semi-log plot of the normalized absorbances for C_6-CPDTO and P3HT

4.3.3 Characterization of the degradation products

UV-Vis absorbance can indicate the progression of photodegradation, but to understand what is happening structurally during photodegradation, we monitored the thin film samples with infrared (IR) spectroscopy. IR spectroscopy can show functional groups present in the polymer, allowing us to see the generation or destruction of particular functional groups during photodegradation.

The IR spectra of P3HT are shown in Figure 4.4 at various times of total illumination under a xenon arc lamp. Alkyl C-H stretching (~2900 cm^{-1}) decreases as illumination time increases, this is a result of degradation of the side chains of the polymer. Degradation of the side chains is known to occur through a radical degradation and has not been reported for singlet oxygen.[32] There is also the appearance of a broad peak around 1700 cm^{-1}, indicative of C=O stretching. The presence of the peak at 1700 cm^{-1} in the 0 min sample is due to aging of the P3HT prior to this study being conducted. A main peak formed at 1728 cm^{-1} (COOH) with shoulder peaks at 1776 (Anhydride) and 1692

cm^{-1} (ketone). Also a broad peak emerged in the region of 1350 – 850 cm^{-1}, which can be assigned to a variety of oxidized sulfur species.[32] A broad absorption peak centered at 3100 cm^{-1} can be attributed to OH stretching of carboxylic acids. Another peak centered at 3460 cm^{-1} indicates OH stretching of an alcohol.

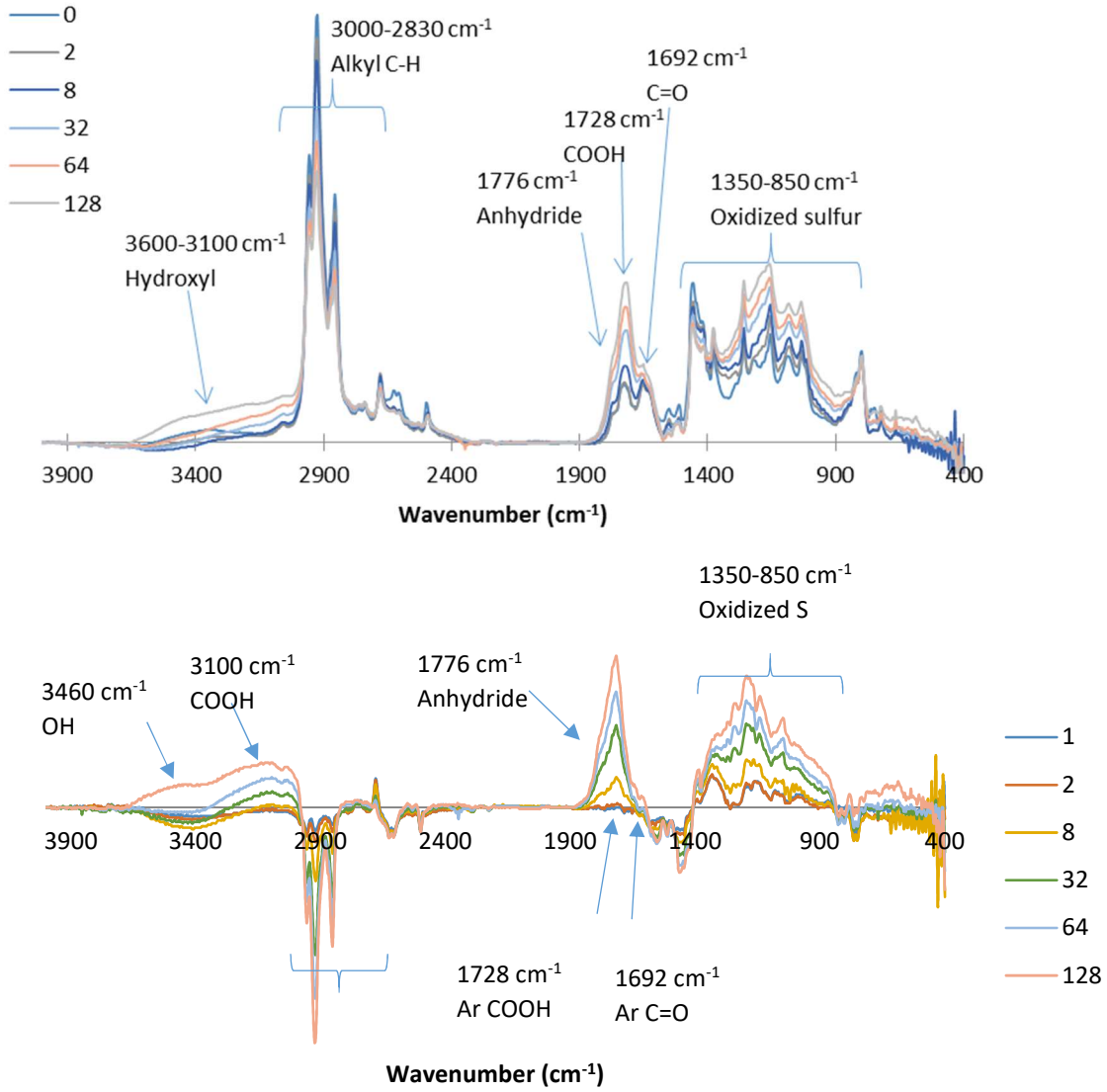

Figure 4.4 IR spectra of P3HT at 0, 30, 60, 120, and 180 minutes of accumulated illumination time (Top) and the same sample with the 0 minute spectrum subtracted (Bottom)

The IR spectra at various times of accumulated illumination time for C_6-CPDTO is shown in Figure 4.5. Similar to P3HT, C_6-CPDTO shows a decrease in alkyl C-H stretching (~2900 cm^{-1}) which indicates the involvement of a radical degradation mechanism While the original carbonyl peak at 1708 cm^{-1} remains constant, a new peak appears at 1724 cm^{-}, is likely due to the original carbonyl in a monomeric unit where S is oxidized (the likelihood of carboxylic acid is eliminated as no hydroxyl peak is seen at ~3400cm^{-1}). It is well known that a carbonyl group substituted with an electron-withdrawing group vibrates at higher frequency.[80] A new peak at 1784 cm^{-1} also appears and this is indicative of a cyclic alkyl ketone, this may be a result of the loss of conjugation in the monomeric unit. Similar to P3HT, absorbance increases in a broad region of 1300-900 cm^{-1} is observed, indicative of the oxidized sulfur species. Unlike P3HT, there is no OH stretching seen in C6-CPDTO.

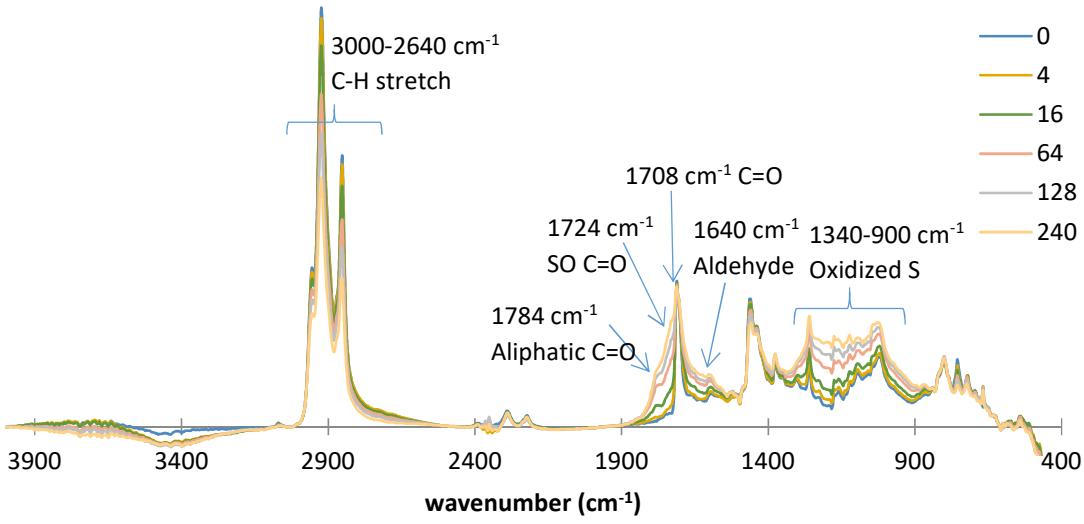

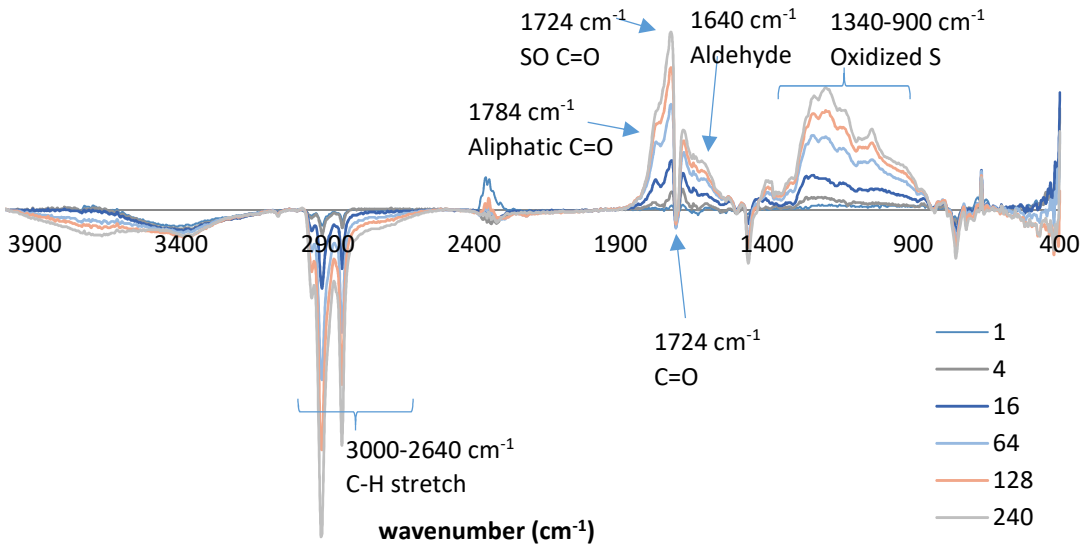

Figure 4.5 IR spectrum for C_6-CPDTO at accumulated times of illumination (Top) IR spectrum with the initial spectrum subtracted (Bottom)

The IR spectrums can give us information on the change in functional groups of the polymers, but for a subtle change like cross linking, IR is unable to detect. Since crosslinking can occur without a change in functional groups, IR isn't efficient at measuring crosslinking. GPC is able to detect the changes in the molecular weight of the polymers that accompany the cross-linking. The samples were degraded on a glass slide and transferred to a vial. The samples were then dissolved in THF and injected into the GPC. Figure 4.6 shows the elugrams for the samples at various total illumination times. P3HT shows a decrease in the peak area of the main peak and the appearance and increase of one peak at a shorter elution time (larger molecular weight). The appearance of larger molecular weight fractions, indicate that cross linking is occurring. The main peak also shifts to longer elution times indicating a decrease in molecular weight. This would typically indicate that chain scission is occurring. Since there is no appearance of peaks corresponding to small molecules in the elugram, chain scission isn't likely.

Another possibility is the loss of rigidity of the polymer causing a decrease in the hydrodynamic volume of P3HT. C_6-CPDTO on the other hand shows a dramatic reduction in the main peak area and a large increase with multiple peaks at shorter retention times, indicating that a large amount of cross-linking is occurring.

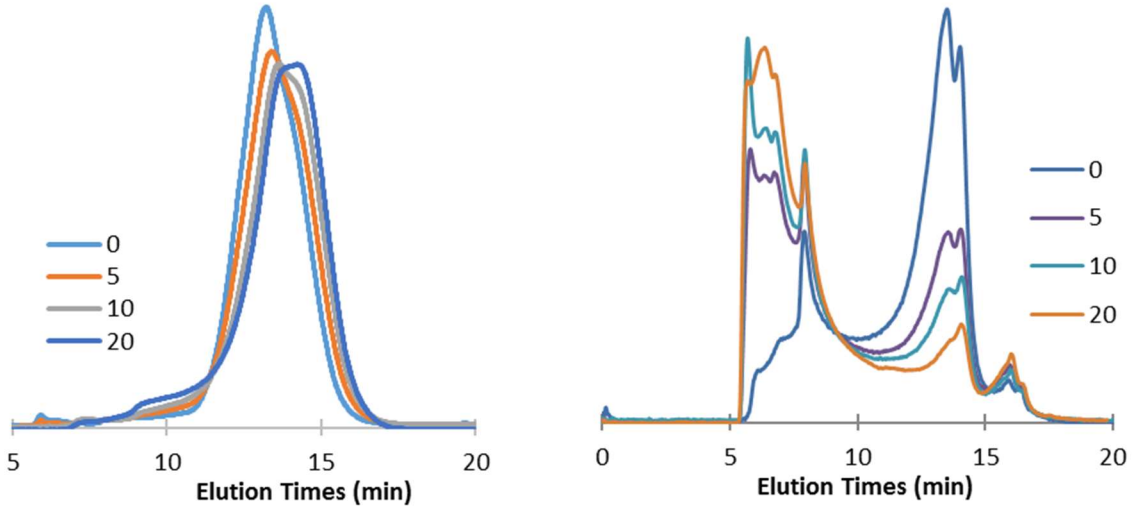

Figure 4.6 IR spectra of P3HT (Left) and C_6-PDTO (Right) at 0, 5, 10, and 20 minutes of accumulated illumination time

To find correlations between polymer cross-linking and backbone photodegradation, the change in the main peak height over time was plotted and compared to the loss in absorbance over time. In P3HT, the loss of absorbance occurs faster than the rate of cross-linking. If you consider that two polymers cross-linking results in the destruction of one double bond, it would suggest that a loss of absorbance in P3HT isn't entirely caused by cross-linking reactions. In C6-CPDTO, the rate of cross-linking is 6 times faster than the rate of absorbance loss, which would indicate that cross-linking is occurring 3 times faster than the destruction of conjugation. This suggests that

in C_6-CPDTO, cross-linking events are occurring that don't involve a double bond, such as radical combination.

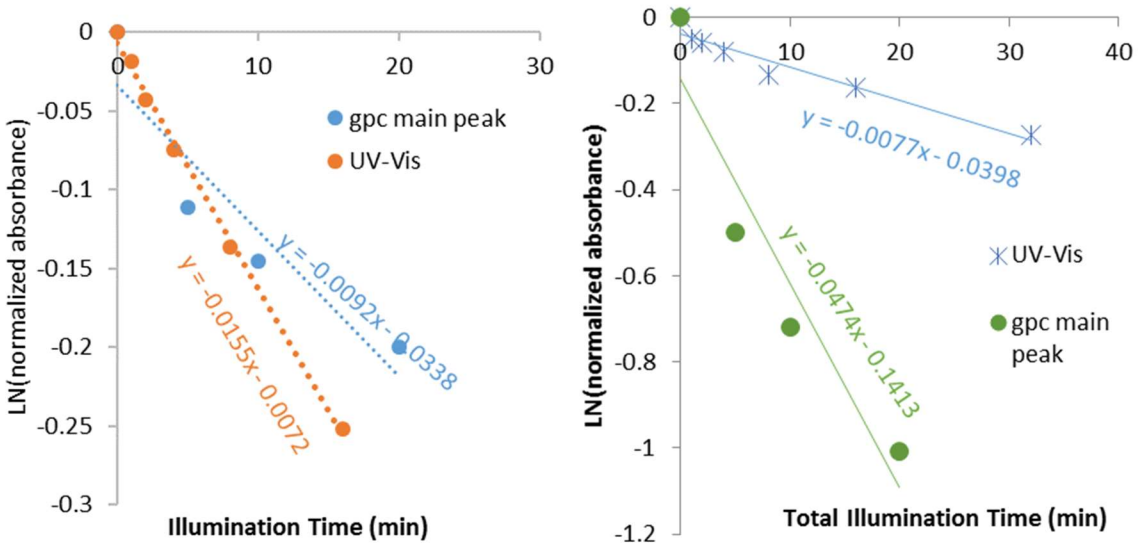

Figure 4.7 UV-vis and GPC main peak intensity vs. accumulated illumination time for P3HT (Left) and C6-CPDTO (Right)

4.3.5 Degradation Mechanisms

Scheme 4.1 P3HT degradation: Radical degradation can result in the oxidation of thiophene (A-D). The loss of aromaticity allows for reactions with singlet oxygen (D-G) or radical addition (D&H).

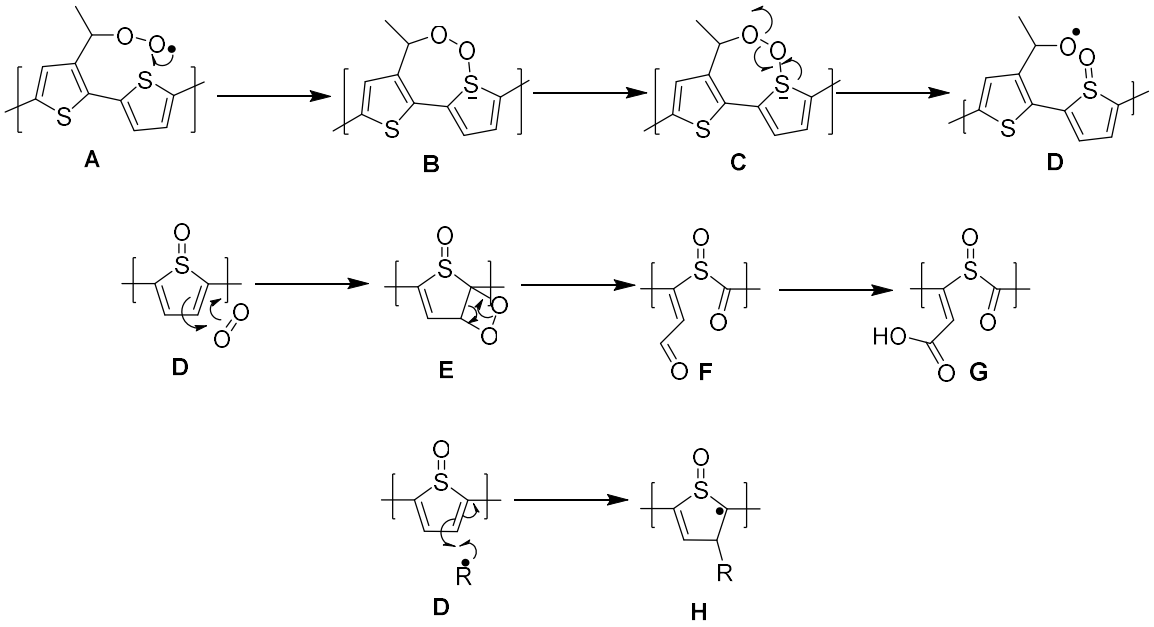

The observation that the C-H IR absorbance decreases for both polymers indicates that the polymers degrade at least in part by a radical degradation mechanism. In this mechanism, radical oxygen anion (O_2^-) abstract a hydrogen atom from the alpha-carbon of the side chain to produce a carbon radical, which reacts with O_2 to give a peroxide (**A**&**I**). The resulting peroxide can either abstract a hydrogen from another polymer chain or oxidize the sulfur of the thiophene ring (**D**&**J**). Henkelmen et al. showed through ab initio calculations that the peroxide is the most likely initiator of sulfur oxidation, and it is unlikely that the peroxide would abstract a hydrogen from another side chain.[75] Scheme 4.1 shows the formation of the transient peroxide ring formed by the attack of the peroxide of the side chain on the lone pair of electrons of the sulfur atom. Oxidation of the sulfur to sulfoxide and sulfone breaks the aromaticity of the thiophene unit as well as introduction of an electron withdrawing moiety. Appearance of oxidized sulfur species is evident in the IR spectra for both P3HT and C_6-CPDTO. The oxidation of sulfur increases the likelihood of radical addition to the double bonds of the thiophene ring. The

radical, denoted by R in Figure 4.1 and 4.2 can be the alkoxy radical, radical oxygen or the side chain alkyl radical. In the case of the alkoxy radical and alkyl radical, radical addition results in cross-linking. The loss of aromaticity also allows for reactions with singlet oxygen. It appears that singlet oxygen plays a role in the photodegradation of P3HT. This is thought to be the case due to the loss of rigidity in the polymer as indicated by gpc and due to the faster loss of absorbance when compared to cross-linking. Singlet oxygen would likely add to the thiophene ring through a 2+2 cycloaddtion (**D**-**E**). This will result in ring opening and the production of a ketone and aldehyde **F**. The aldehyde can then be oxidized to carboxylic acid **G**. This accounts for the carboxylic acid observed in the IR of photodegraded P3HT.

Scheme 4.2 Peroxide (I) formed during initiation, oxidizes thiophene to produce (J). once aromaticity is broken, cross-linking (Kto L) becomes more likely.

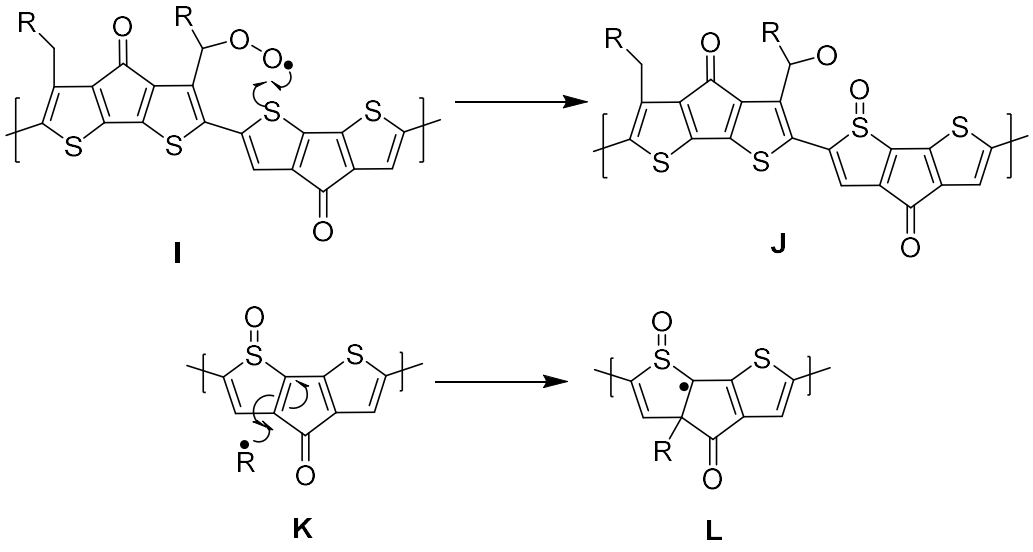

The extent of side chain degradation appears to be similar for both P3HT and C_6-CPDTO. Manceau et al. showed that the radical degradation of the side chains of P3HT could produce carboxylic acids.[32] The degradation of the side chains for both P3HT and C_6-CPDTO is expected to be the same, but no carboxylic acids are noted in the degradation of C_6-CPDTO. Henkelman et al. have indicated that it is unfavorable for the peroxide radical **A** in Figure 4.1 to abstract a hydrogen from another polymer chain to form the hydroperoxide.[75] The oxygen radical species **D**. that remains after oxidation of the thiophene ring can undergo beta-scission producing an aldehyde **M.** The aldehyde reacts readily with a radical initiator, in this case, either superoxide radical anion or a previously generated radical. The radical can abstract a hydrogen from the aldehyde **M** to produce an acyl radical **N**. The acyl radical loses carbon monoxide to form an aryl radical **O** which then abstracts a hydrogen to propagate the radical mechanism and forms **P.** This mechanism occurs in both polymers and is responsible for the loss of side chains.

Scheme 4.3 Proposed side chain degradation with

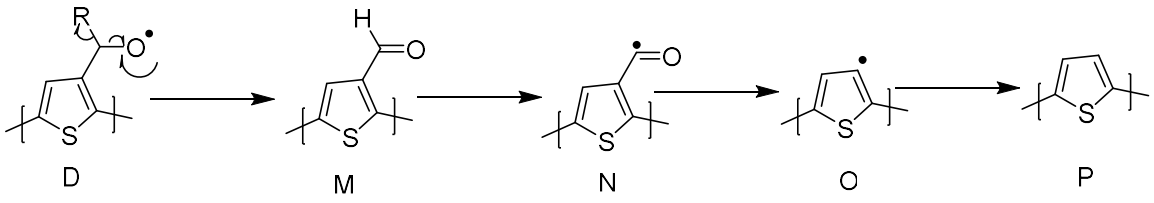

4.4 Conclusion

The initiation of photodegradation in both P3HT and C_6-CPDTO is the formation of radicals on the side chains of the polymers. After radical degradation is initiated, generated radicals react with the conjugated backbone of the polymers, destroying the π conjugation resulting in the loss of absorbance. The attack on the π bonds often resuts in

crosslinking of the polymers. Although both polymers degrade by radical degradation, the IR spectra of the degraded products look different for P3HT and C_6-CPDTO. Previous reports have stated that P3HT degrades by a radical mechanism only, this report suggests that singlet oxygen plays a role in the degradation of P3HT. This action by singlet oxygen accounts for the difference between degradation mechanisms for these polymers.

Chapter 5 Summary

This study has aimed to gain a better understanding of how conjugated polymers degrade when exposed to light. Photostability is an important issue when designing a device, as it directly effects the useful lifetime of the device. In this study, only the photochemical stability of the conjugated polymers was considered. There are other factors that affect the stability of a device, including; morphology changes and electrode oxidation. These issues vary among applications, but the stability of the active layer is a universal problem.

Our previous work had shown that there was a correlation between the LUMO energy level and the photostability of PPV polymers. It was shown that through the addition of cyano substituents to the vinylene unit of the polymer that the LUMO level could be lowered, and by lowering the LUMO level the photostability of the polymers increased. To further this, in this investigation, the alkoxy side chains of RO-diCN-PPV were replaced with alkyl side chains to produce C8-diCN-PPV. The replacement of the side chains was aimed at lowering the LUMO level even further. Despite having a lower LUMO level then RO-diCN-PPV, C8-diCN-PPV was less photostable. The mechanisms that were acting on these polymers during photodegradation were investigated to gain a better understanding of the structure-photostability relationship. It was discovered that unlike other PPV polymers, RO-diCN-PPV and C8-diCN-PPV both photodegrade through a singlet oxygen mechanism. This is due to the fact that the LUMO level of C8-diCN-PPV is lower than the LUMO level of O_2, and the LUMO level of RO-diCN-PPV is not high enough to permit efficient generation of superoxide anion. What makes RO-diCN-PPV more photostable than C8-diCN-PPV, is the slower rate of intersystem crossing in RO-diCN-PPV, which decreases the rate of singlet oxygen generation.

Since, it was determined that RO-diCN-PPV and C8-diCN-PPV primarily were photo-oxidized by singlet oxygen, stabilization was attempted through the addition of a well-known singlet oxygen quencher, DABCO. When DABCO was doped into a film of C8-diCN-PPV at 15 mol%, it decreased the rate of photo-oxidation. When DABCO was added to RO-diCN-PPV, the rate of photo-oxidation increased. The photodegradation mechanisms of the diCN-PPV polymers doped with DABCO were studied. It was observed that DABCO was very efficient at quenching singlet oxygen in the C8-diCN-PPV films. In RO-diCN-PPV films, DABCO initiates a radical degradation mechanism through a one electron transfer from the HOMO of DABCO to a hole in the HOMO of an excited RO-diCN-PPV polymer. This doesn't occur in the C8-diCN-PPV films due to the large gap between the HOMO levels of C8-diCN-PPV and DABCO.

Finally, a comparative study on the photostability of two polythiophene polymers, P3HT and C_6-CPDTO was conducted. These two polymers have structural similarities and only vary by a few details. In general, C_6-CPDTO has a lower LUMO level compared to P3HT and fewer side chains. These differences indeed make C_6-CPDTO more stable. Investigation into the photodegradation mechanisms revealed that C_6-CPDTO and P3HT degrade through a radical mechanism. While previous reports had indicated that P3HT only degrades by a radical degradation mechanism, our study indicates that singlet oxygen likely plays a role. Further research is needed to fully characterize the role of singlet oxygen in the degradation of P3HT.

REFERENCES

1. Li, Gang; Zhu, Rui; Yang, Yang, *Nat. Photonics* **2012,** *6* (3), 153-161.

2. Gunes, Serap; Neugebauer, Helmut; Sariciftci, Niyazi Serdar, *Chem Rev* **2007,** *107* (4), 1324-38.

3. Ward, Jeremy W.; Lamport, Zachary A.; Jurchescu, Oana D., *ChemPhysChem* **2015,** *16* (6), 1118-1132.

4. Chou, Ying-Hsuan; Chang, Hsuan-Chun; Liu, Cheng-Liang; Chen, Wen-Chang, *Polym. Chem.* **2015,** *6* (3), 341-352.

5. Perepichka, Dmitrii F.; Perepichka, Igor F.; Meng, Hong; Wudl, Fred, *Opt. Sci. Eng.* **2007,** *111* (Organic Light-Emitting Materials and Devices), 45-293.

6. Wu, Hongbin; Ying, Lei; Yang, Wei; Cao, Yong, *Chem. Soc. Rev.* **2009,** *38* (12), 3391-3400.

7. Al Salhi, Mohamad Saleh; Alam, Javed; Dass, Lawrence Arockiasamy; Raja, Mohan, *Int. J. Mol. Sci.* **2011,** *12*, 2036-2054.

8. Duran-Sampedro, Gonzalo; Agarrabeitia, Antonia R.; Garcia-Moreno, Inmaculada; Costela, Angel; Banuelos, Jorge; Arbeloa, Teresa; Lopez Arbeloa, Inigo; Chiara, Jose Luis; Ortiz, Maria J., *Eur. J. Org. Chem.* **2012,** *2012* (32), 6335-6350.

9. Navarro-Fuster, Victor; Calzado, Eva M.; Boj, Pedro G.; Quintana, Jose A.; Villalvilla, Jose M.; Diaz-Garcia, Maria A.; Trabadelo, Vera; Juarros, Aritz; Retolaza, Aritz; Merino, Santos, *Appl. Phys. Lett.* **2010,** *97* (17), 171104/1-171104/3.

10. Kaeser, Adrien; Schenning, Albertus P. H. J., *Adv. Mater. (Weinheim, Ger.)* **2010,** *22* (28), 2985-2997.

11. Li, Kai; Liu, Bin, *Polym. Chem.* **2010,** *1* (3), 252-259.

12. Li, Kai; Liu, Bin, *Journal of Materials Chemistry* **2012,** *22* (4), 1257-1264.

13. Duan, Xinrui; Liu, Libing; Feng, Fude; Wang, Shu, *Acc. Chem. Res.* **2010,** *43* (2), 260-270.

14. Feng, Xuli; Liu, Libing; Wang, Shu; Zhu, Daoben, *Chem. Soc. Rev.* **2010,** *39* (7), 2411-2419.

15. Alvarez, Adrian; Costa-Fernandez, Jose M.; Pereiro, Rosario; Sanz-Medel, Alfredo; Salinas-Castillo, Alfonso, *TrAC, Trends Anal. Chem.* **2011,** *30* (9), 1513-1525.

16. Kim, Ha Na; Ren, Wen Xiu; Kim, Jong Seung; Yoon, Juyoung, *Chem. Soc. Rev.* **2012,** *41* (8), 3210-3244.

17. Kim, Ha Na; Guo, Zhiqian; Zhu, Weihong; Yoon, Juyoung; Tian, He, *Chem. Soc. Rev.* **2011,** *40* (1), 79-93.

18. Hu, Jinming; Liu, Shiyong, *Macromolecules (Washington, DC, U. S.)* **2010,** *43* (20), 8315-8330.

19. Inzelt, György, Introduction. In *Conducting Polymers: A New Era in Electrochemistry*, Inzelt, G., Ed. Springer Berlin Heidelberg: Berlin, Heidelberg, 2012; pp 1-6.

20. MacDiarmid, Alan G., *Angewandte Chemie International Edition* **2001,** *40* (14), 2581-2590.

21. Shirakawa, Hideki; Louis, Edwin J.; MacDiarmid, Alan G.; Chiang, Chwan K.; Heeger, Alan J., *Journal of the Chemical Society, Chemical Communications* **1977,** (16), 578-580.

22. AB, Nobel Media The Nobel Prize in Chemistry 2000. http://www.nobelprize.org/nobel_prizes/chemistry/laureates/2000/index.html (accessed 07/10).

23. Coropceanu, Veaceslav; Cornil, Jérôme; da Silva Filho, Demetrio A.; Olivier, Yoann; Silbey, Robert; Brédas, Jean-Luc, *Chemical Reviews* **2007,** *107* (4), 926-952.

24. Hoke, Eric T.; Sachs-Quintana, I. T.; Lloyd, Matthew T.; Kauvar, Isaac; Mateker, William R.; Nardes, Alexandre M.; Peters, Craig H.; Kopidakis, Nikos; McGehee, Michael D., *Adv. Energy Mater.* **2012,** *2* (11), 1351-1357.

25. Bundgaard, Eva; Helgesen, Martin; Carle, Jon E.; Krebs, F. C.; Jorgensen, Mikkel, *Macromol. Chem. Phys.* **2013,** *214*, 1546-1558.

26. Sun, Jianyuan; Sanow, Logan P.; Sun, Sam-Shajing; Zhang, Cheng, *Macromolecules (Washington, DC, U. S.)* **2013,** *46* (11), 4247-4254.

27. Corazza, Michael; Krebs, Frederik C.; Gevorgyan, Suren A., *Sol. Energy Mater. Sol. Cells* **2015,** *143*, 467-472.

28. M. Manceau, A. Rivaton, J. L. Gardette, *Stability and Degradation of Organic and Polymer Solar Cells*. John Wiley & Sons, Ltd.: 2012.

29. Cao, Huanqi; He, Weidong; Mao, Yiwu; Lin, Xiao; Ishikawa, Ken; Dickerson, James H.; Hess, Wayne P., *J. Power Sources* **2014,** *264*, 168-183.

30. Chambon, Sylvain; Rivaton, Agnes; Gardette, Jean-Luc; Firon, Muriel, *Polym. Degrad. Stab.* **2011,** *96* (6), 1149-1158.

31. Chambon, Sylvain; Rivaton, Agnes; Gardette, Jean-Luc; Firon, Muriel, *J. Polym. Sci., Part A: Polym. Chem.* **2009,** *47* (22), 6044-6052.

32. Manceau, Matthieu; Rivaton, Agnes; Gardette, Jean-Luc; Guillerez, Stephane; Lemaitre, Noella, *Polym. Degrad. Stab.* **2009,** *94* (6), 898-907.

33. Dam, Niels; Scurlock, Rodger D.; Wang, Bojie; Ma, Lichuan; Sundahl, Mikael; Ogilby, Peter R., *Chem. Mater.* **1999,** *11* (5), 1302-1305.

34. Moslin, Ryan M.; Andrew, Trisha L.; Kooi, Steven E.; Swager, Timothy M., *J. Am. Chem. Soc.* **2009,** *131* (1), 20-21.

35. Liu, Y.; Liu, M. S.; Jen, A. K. Y., *Acta Polym.* **1999,** *50* (2-3), 105-108.

36. Brehm, Isabella; Hinneschiedt, Sabine; Meier, Herbert, *Eur. J. Org. Chem.* **2002,** (18), 3162-3170.

37. Yeh, Hsiu-Chih; Wu, Wei-Ching; Wen, Yuh-Sheng; Dai, De-Chang; Wang, Juen-Kai; Chen, Chin-Ti, *J. Org. Chem.* **2004,** *69* (19), 6455-6462.

38. Yamashita, Yoichiro; Endo, Takeshi, *J. Appl. Polym. Sci.* **2005,** *98* (1), 466-473.

39. Taylor, Edward C.; Andrade, Juan G.; John, K. Chacko; McKillop, Alexander, *J. Org. Chem.* **1978,** *43* (11), 2280-2.

40. Ester Formation and Hydrolysis and Related Reaction. In *Comprehensive chemical kinetics* Bamford, C. H.; Tipper, C. F. H.; Compton, R. G., Eds. Amsterdam, New York, Elsevier Pub. Co., 1969-<1985 >: 1969.

41. Murray, Robert Wallace; Wasserman, Harry H., *Singlet oxygen*. New York : Academic Press, 1979.: 1979.

42. Williams, G. V. M.; Kutuvantavida, Y.; Janssens, S.; Raymond, S. G.; Do, My T. T.; Bhuiyan, M. D. H.; Quilty, J. W.; Denton, N.; Kay, A. J., *Journal of Applied Physics* **2011,** *110* (8), 083524.

43. Steiner, Ulrich; Winter, Gerhard; Kramer, Horst E. A., *J. Phys. Chem.* **1977,** *81* (11), 1104-10.

44. Kaise, Masahiro; Someno, Kazuo, *Chemistry Letters* **1987,** *16* (7), 1295-1298.

45. Zheng, Zi-Rong; Evans, Dennis H.; Nelsen, Stephen F., *J. Org. Chem.* **2000,** *65* (6), 1793-1798.

46. Scurlock, Rodger D.; Wang, Bojie; Ogilby, Peter R.; Sheats, James R.; Clough, Roger L., *J. Am. Chem. Soc.* **1995,** *117* (41), 10194-202.

47. Manceau, Matthieu; Bundgaard, Eva; Carle, Jon E.; Hagemann, Ole; Helgesen, Martin; Sondergaard, Roar; Jorgensen, Mikkel; Krebs, Frederik C., *J. Mater. Chem.* **2011,** *21* (12), 4132-4141.

48. Tromholt, Thomas; Madsen, Morten Vesterager; Carle, Jon E.; Helgesen, Martin; Krebs, Frederik C., *J. Mater. Chem.* **2012,** *22* (15), 7592-7601.

49. Kutuvantavida, Yasar; Williams, Grant V. M.; Bhuiyan, M. Delower H.; Raymond, Sebastiampillai G.; Kay, Andrew J., *J. Phys. Chem. C* **2015,** *119* (6), 3273-3278.

50. Foucher, C.; Guilhabert, B.; Herrnsdorf, J.; Laurand, N.; Dawson, M. D., *Opt. Express* **2014,** *22* (20), 24160-24168.

51. Moretti, Elisa; Talon, Aldo; Storaro, Loretta; Le Donne, Alessia; Binetti, Simona; Benedetti, Alvise; Polizzi, Stefano, *J. Lumin.* **2014,** *146*, 178-185.

52. Chambon, Sylvain; Rivaton, Agnès; Gardette, Jean-Luc; Firon, Muriel; Lutsen, Laurence, *Journal of Polymer Science Part A: Polymer Chemistry* **2007,** *45* (2), 317-331.

53. Sanow, Logan P.; Sun, Jianyuan; Zhang, Cheng, *J. Polym. Sci., Part A: Polym. Chem.* **2015,** *53* (24), 2820-2828.

54. Moura, J. C. V. P.; Oliveira-Campos, A. M. F.; Griffiths, J., *Dyes Pigm.* **1997,** *33* (3), 173-196.

55. Tian, Zhiyuan; Yu, Jiangbo; Wang, Xiaoli; Groff, Louis C.; Grimland, Jennifer L.; McNeill, Jason D., *J. Phys. Chem. B* **2013,** *117* (16), 4517-4520.

56. Ouannes, Catherine; Wilson, Therese, *J. Amer. Chem. Soc.* **1968,** *90* (23), 6527-8.

57. Valnes, Kolbjoern; Brandtzaeg, Per, *J. Histochem. Cytochem.* **1985,** *33* (8), 755-61.

58. Ogryzlo, Elmer A.; Tang, C. W., *J. Amer. Chem. Soc.* **1970,** *92* (17), 5034-6.

59. Packer, J. E.; Mahood, J. S.; Mora-Arellano, V. O.; Slater, T. F.; Willson, R. L.; Wolfenden, B. S., *Biochem. Biophys. Res. Commun.* **1981,** *98* (4), 901-6.

60. Yosef, H. A. A.; Morsy, N. M.; Mahran, M. R. H.; Aboul-Enein, H. Y., *J. Iran. Chem. Soc.* **2007,** *4* (1), 46-58.

61. Vasudevan, D.; Wendt, H., *J. Electroanal. Chem.* **1995,** *392* (1-2), 69-74.

62. Hasegawa, Eietsu; Tosaka, Emi; Yoneoka, Akira; Tamura, Yukinobu; Takizawa, Shin-ya; Tomura, Masaaki; Yamashita, Yoshiro, *Res. Chem. Intermed.* **2013,** *39* (1), 247-267.

63. Hasegawa, Eietsu; Ishiyama, Kenyuki; Fujita, Takayuki; Kato, Tomoyasu; Abe, Toshiaki, *J. Org. Chem.* **1997,** *62* (8), 2396-2400.

64. Chow, Yuan L.; Danen, Wayne C.; Nelsen, Stephen F.; Rosenblatt, David H., *Chem. Rev.* **1978,** *78* (3), 243-74.

65. Dinnocenzo, J. P.; Banach, T. E., *J. Am. Chem. Soc.* **1989,** *111* (23), 8646-53.

66. Gardette, Jean-Luc; Mailhot, Benedicte; Posada, Fabrice; Rivaton, Agnes; Wilhelm, Catherine, *Macromol. Symp.* **1999,** *143* (World Polymer Congress, 37th International Symposium on Macromolecules, 1998), 95-109.

67. Zytowski, Torsten; Fischer, Hanns, *J. Am. Chem. Soc.* **1996,** *118* (2), 437-9.

68. Zhao, Jingbo; Li, Yunke; Yang, Guofang; Jiang, Kui; Lin, Haoran; Ade, Harald; Ma, Wei; Yan, He, *Nature Energy* **2016,** *1*, 15027.

69. Aoyama, Yoshinori; Yamanari, Toshihiro; Ohashi, Noboru; Shibata, Yosei; Suzuki, Yasumasa; Mizukado, Junji; Suda, Hiroyuki; Yoshida, Yuji, *Sol. Energy Mater. Sol. Cells* **2014,** *120* (PB), 584-590.

70. Lambert, Tim L.; Ferraris, John P., *J. Chem. Soc., Chem. Commun.* **1991,** (11), 752-4.

71. Wang, Hsing-Ju; Chou, Chen-Wei; Chen, Chih-Ping; Chen, Ying-Hsiao; Lee, Rong-Ho; Jeng, Ru-Jong, *J. Mater. Chem. A* **2013,** *1* (31), 8950-8960.

72. Chen, Liang; Mizukado, Junji; Suzuki, Yasumasa; Kutsuna, Shuzo; Aoyama, Yoshinori; Yoshida, Yuji; Suda, Hiroyuki, *Chem. Phys. Lett.* **2014,** *605-606*, 98-102.

73. Chen, Liang; Yamane, Shogo; Mizukado, Junji; Suzuki, Yasumasa; Kutsuna, Shuzo; Uchimaru, Tadafumi; Suda, Hiroyuki, *Chem. Phys. Lett.* **2015,** *624*, 87-92.

74. Manceau, Matthieu; Rivaton, Agnes; Gardette, Jean-Luc, *Macromol. Rapid Commun.* **2008,** *29* (22), 1823-1827.

75. Sai, Na; Leung, Kevin; Zador, Judit; Henkelman, Graeme, *Phys. Chem. Chem. Phys.* **2014,** *16* (17), 8092-8099.

76. Holdcroft, Steven, *Macromolecules* **1991,** *24* (17), 4834-8.

77. Abdou, Mohamed S. A.; Holdcroft, Steven, *Macromolecules* **1993,** *26* (11), 2954-62.

78. Hintz, H.; Egelhaaf, H. J.; Peisert, H.; Chasse, T., *Polym. Degrad. Stab.* **2010,** *95* (5), 818-825.

79. Abdou, Mohamed S. A.; Holdcroft, Steven, *Canadian Journal of Chemistry* **1995,** *73* (11), 1893-1901.

80. Silverstein, Robert M.; Webster, Francis X.; Kiemle, David J., *Spectrometric identification of organic compounds*. Hoboken, NJ : John Wiley & Sons, c2005. 7th ed. / Robert M. Silverstein, Francis X. Webster, David J. Kiemle.: 2005.